4 Results

4.1 Crystal structure determination of RuvBL1

4.1.1 Purification of RuvBL1

RuvBL1 carried a 6xHis and a FLAG tag at the N terminus and was purified in two steps. The purification is shown exemplarily for selenomethionine (Se-Met) substituted RuvBL1, which was used for structure determination. First the 6xHis tagged protein was loaded onto a Ni-NTA Superflow (QIAGEN) column and eluted in a gradient with rising imidazole concentration between 80 and 200 mM imidazole (Figure 7).

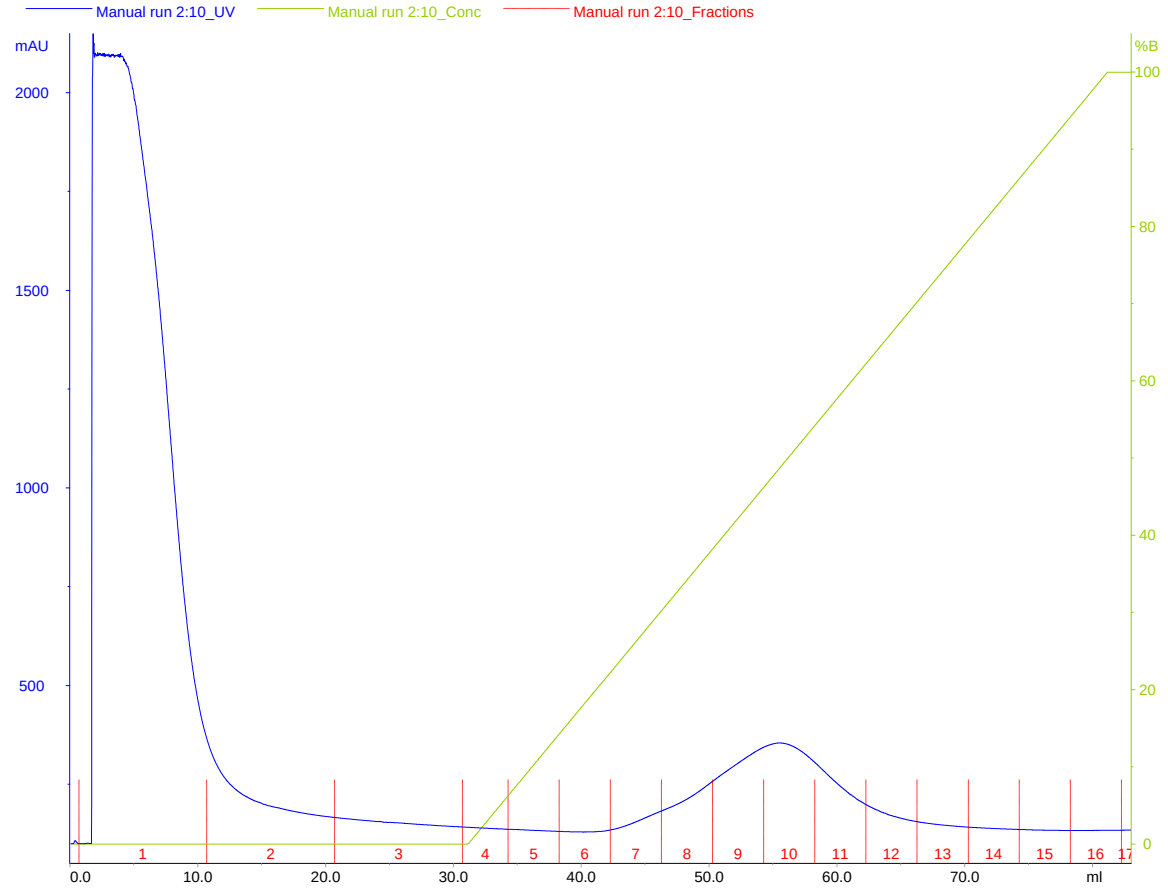

Figure 7: Ni-NTA chromatography profile of Se-Met substituted RuvBL1. The 6xHis tagged protein (blue peak) was eluted in a gradient from 20-400 mM imidazole. Fractions 8-11 contained the purified protein. The green curve indicates the percentage of buffer B and therefore the amount of imidazole during elution, while the blue curve shows the protein absorption at 280 nm.

Protein containing fractions 8-11 were pooled and loaded onto a MonoQ anion exchange column. RuvBL1 eluted in a gradient with rising NaCl concentration between 125 and 150 mM NaCl (Figure 8).

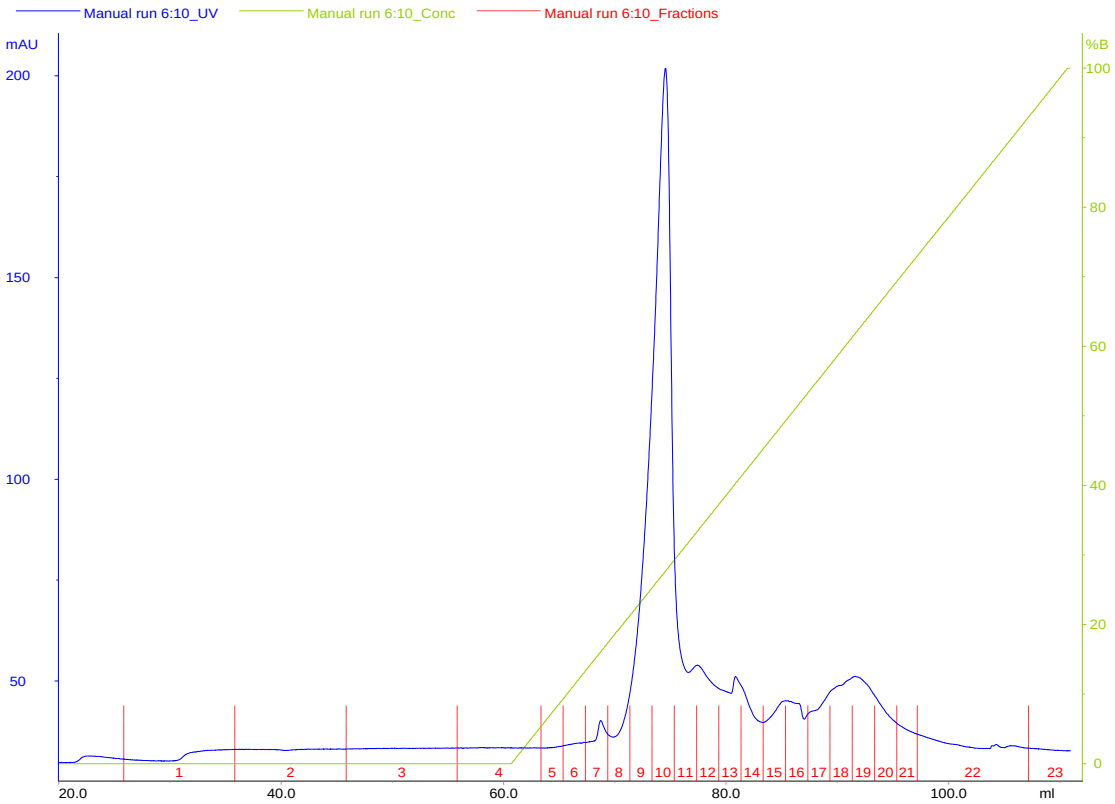

Figure 8: Anion exchange chromatography profile of Se-Met substituted RuvBL1. RuvBL1 eluted in a gradient with rising NaCl concentration between 125 and 150 mM NaCl. Fractions 9 and 10 contained the purified protein. The green curve indicates the percentage of buffer B and therefore the amount of NaCl, while the blue curve shows the protein absorption at 280 nm.

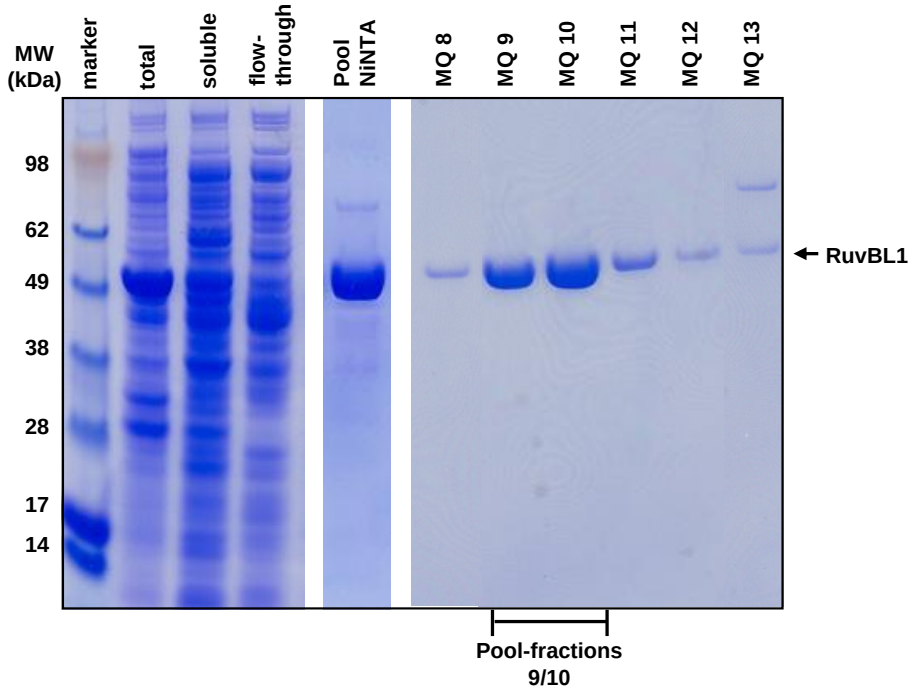

Figure 9: SDS-PAGE of Se-Met substituted RuvBL1 purification. Following cell disruption (total) the soluble proteins were loaded onto a Ni-NTA column. In the second purification step (MonoQ) all impurities contained in the Ni-NTA pool (Pool Ni-NTA) were eliminated (MQ13) and the pure fractions MQ 9 and 10 were used for crystallization.

The SDS-PAGE in Figure 9 shows that all impurities were eliminated in the anion exchange chromatography. Pure MonoQ fractions 9 and 10 were pooled, concentrated to a final concentration of 15 mg/ml and used for crystallization studies (see 4.1.2). Analytical gel filtration and DLS experiments showed that RuvBL1 is predominantly a monomer at lower concentrations (1.5 mg/ml) and a hexamer at concentrations above 7 mg/ml (data not shown). In addition the oligomerisation of RuvBL1 was analysed in detail using small-angle x-ray scattering (see chapter 4.4).

4.1.2 Crystallization of RuvBL1

Searching for initial crystallization conditions of RuvBL1 the best hit was found for the condition C2 of the Malonate Screen (Hampton Research) corresponding to a solution composition of 1.5 M sodium malonate pH 6.0 without any other additives. The results were reproducible at the microliter scale using the hanging drop vapour-diffusion method, with a drop composition of 1.5 µl of protein solution (15 mg/ml in 20 mM Tris-HCl pH 8.0, 10 % glycerol, 150 mM NaCl and 2 mM β-mercaptoethanol) and 1.5 µl of reservoir solution, equilibrated against 500 µl of precipitant solution in the well. Crystallization conditions were optimised by performing a gradient with increasing sodium malonate concentrations at pH 6. The best crystals were obtained from a solution containing 1.6 M sodium malonate pH 6 at 293 K (Figure 10). The crystals were hexagonal and appeared after two days with size dimensions of approximately 160 x 60 µm.

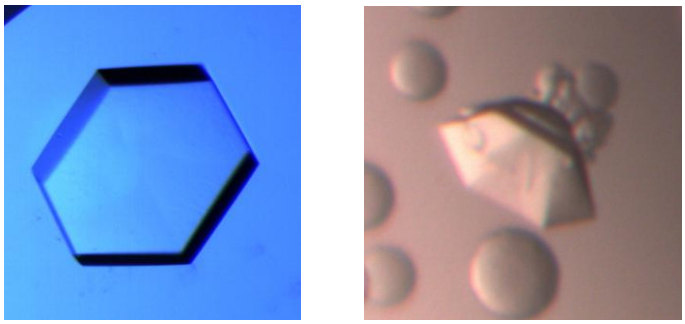

A) Native B) Se-Met

Figure 10: A, Crystal of native RuvBL1. B, Crystal of Se-Met substituted RuvBL1.

A crystal of the Se-Met derivative obtained under these conditions (Figure 10B) was used to measure diffraction data leading to structure determination (Figure 11). All data sets were collected at the European Synchrotron Radiation Facility (ESRF) in Grenoble at beamline ID14-4 using an ADSC Quantum 4 detector at a wavelength corresponding to the maximal value of f” from the Se atoms near the x-ray absorption K-edge.

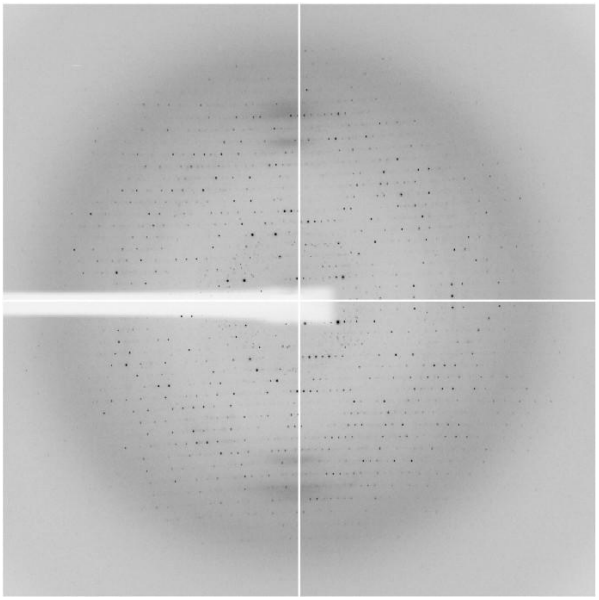

Figure 11: Diffraction pattern of Se-Met substituted RuvBL1. The crystal diffracted to 2.2 Å resolution and belonged to the space group *P*6.

		RuvBL1 Se-Met		
Data collection				
Space group		P6		
Cell dimensions(Å)				
	a	207.2		
	c	60.77		
		peak		
Wavelength (Å)		0.9791		
Resolution (Å)		45.4-2.2 (2.32-2.20)		
R_{merge}		0.068 (0.617)		
$I / \sigma (I)$		8.1 (1.2)		
Observations (unique refl.)		612,942 (73,593)		
Completeness (%)		96.5 (80.0)		
Redundancy		8.3 (3.8)		
Estimated $B_{overall}$ ($Å^2$)		41.1		
Refinement				
Resolution (Å)		45.4 – 2.2		
No. reflections		70028		
R_{work} / R_{free}		0.206 / 0.257		
No. Atoms				
Protein		8,454		
ADP		81		
Water		158		
Average *B*-factors		Monomer A	Monomer B	Monomer C
Protein main-chain (side-chain)		47.3 (51.3)	56.1 (59.4)	64.1 (66.5)
ADP		27.2	35.5	47.1
Water			47.1	
R.m.s deviations				
Bond lengths (Å)		0.014		
Bond angles (°)		1.48		

Table 9: Data collection, phasing and refinement statistics for RuvBL1. Highest resolution shell is shown in parenthesis. R-free is calculated from a random sample containing 5 % of the total number of independent reflections measured. B-factors calculated from equivalent isotropic B values, including the Translation/Libration Screw (TLS) contribution for the protein atoms.

The hexagonal crystals belonged to the space group *P*6 with unit-cell parameters a = b = 207.1 Å, c = 60.7 Å, with three molecules in the asymmetric unit. A summary of the data collection statistics is listed in Table 9.

4.1.3 Structure of the RuvBL1 monomer

The crystal structure of RuvBL1 was solved from the *P*6 crystal form with data at 2.2 Å resolution (Gorynia et al. 2006), showing a hexamer, where each monomer appears complexed with one ADP molecule. The RuvBL1 monomer has approximate dimensions of 75 x 55 x 45 Å and contains 14 α-helices, 16 β-strands and two 3_{10}-helices (Figure 12A and B). These structural elements fold into three domains (DI, DII and DIII; Figure 12B). DI consists of amino acids 1-120 and 296-365 with DII inserted in-between and contains 6 α-helices (α1−α4; α1'; α5'), 9 β-strands (β1-β5; β1'-β4') and 2 very short 3_{10}-helices. This domain is a triangle-shaped nucleotide-binding domain with a Rossmann-like α/β/α fold composed of a core β-sheet consisting of five parallel β-strands with two flanking α-helices on each side (Figure 12B). The loop between β1 and α2 is the conserved P-loop (Walker A motif) which functions to bind and orient the γ-phosphate of ATP for hydrolysis. In addition, the conserved Walker B motif as well as the sensor 1 and the Arginine finger for the adjacent molecule in the hexamer are also present. The core five-stranded β-sheet of the Rossmann-like α/β/α fold is similar to the AAA^+ module of other family members, such as RuvB (branch migration) (Putnam et al. 2001), NSF-D2 (membrane fusion) (Lenzen et al. 1998), SV40 large tumour antigen (replication of viral DNA) (Enemark and Joshua-Tor 2006; Gai et al. 2004; Li et al. 2003), the AAA^+ domain of PspF (transcription activation) (Rappas et al. 2006) and the hexameric ATPase P4 of dsRNA bacteriophage ϕ12 (RNA packaging inside the virus capsid) (Mancini et al. 2004). A succinct structural comparison between the Rossmann fold (DI) of RuvBL1 and that of other AAA^+ proteins is shown in Table 10.

A striking difference, however, is that in RuvBL1 the Walker A and Walker B motifs are separated by 174 amino acids whereas they are closely spaced in the other molecules. This 174 amino acid residue insertion between α3 and β3 (Figure 12A and B) constitutes the novel domain (DII), which appears to be unique to RuvBL1 by database searches (Putnam et al. 2001). A three-dimensional structure search in the DALI server (Holm and Sander 1993) revealed that the spatial arrangement of the seven β-strands (β6-β12) resembles that of the DNA-binding domains of different proteins involved in DNA metabolism, such as the highly conserved eukaryotic protein RPA (replication protein A, PDB 1JMC).

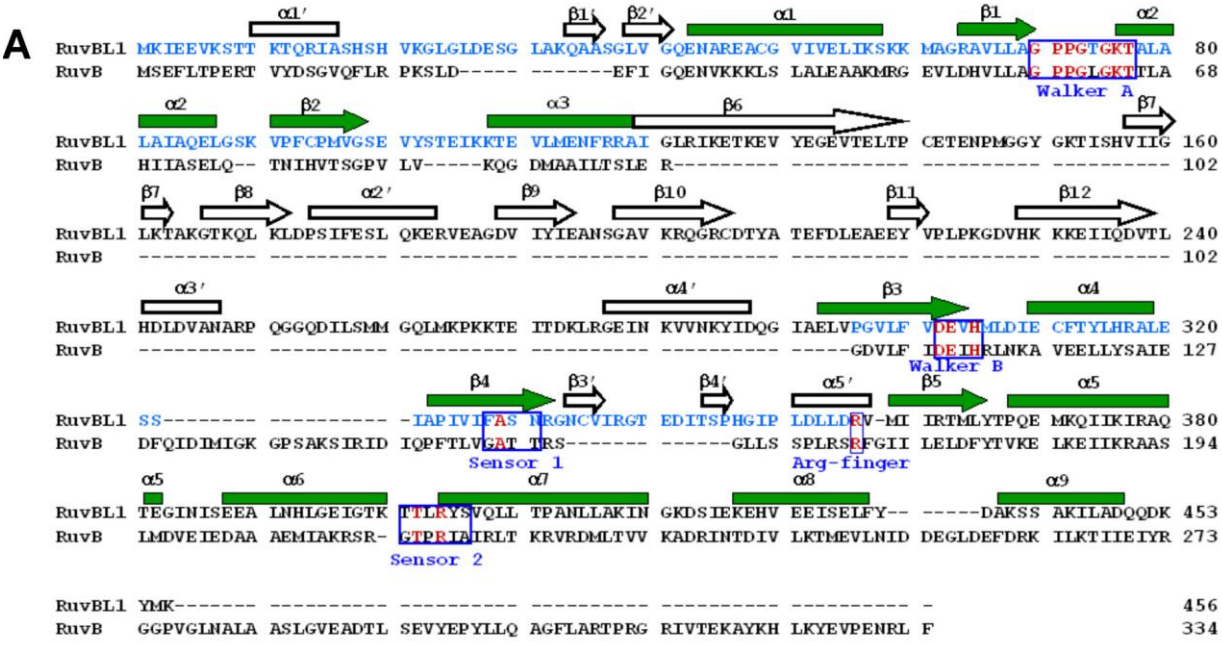

Figure 12: Sequence alignment and three-dimensional structures of RuvBL1 and RuvB. A, Amino acid sequences of RuvBL1 and *Thermotoga maritima* RuvB were aligned by structural superposition on a three-dimensional graphics workstation. The secondary structure elements represented in green are common to both RuvB and RuvBL1. The numbering scheme followed was adopted in order to keep the numbering of secondary structure features consistent between RuvB and RuvBL1. Amino acid residues in RuvBL1 DI are represented in light blue. Conserved residues in the nucleotide-binding motifs of both molecules are coloured red. B, Ribbon diagram of the RuvBL1 monomer showing its domain structure. The ADP molecule is depicted in space-filling mode, where each atom is represented by a sphere with a diameter twice its conventional van der Waals radius. Carbon, nitrogen, oxygen and phosphorus atoms are coloured grey, blue, red and green, respectively; C, Ribbon diagram of the superposed *Thermotoga maritima* RuvB monomer (PDB 1IN7) showing its domain structure. In B and C equivalent domains in RuvBL1 and RuvB are represented in the same colour. Panels B and C were prepared with DINO (Philippsen 2002).

Molecule name	PDB code	Quaternary structure in crystal	Walker A Region	r.m.s.d. C^{α}	Number of C^{α} fit in DI
RuvBL1	2C9O	Hexamer	GPPGT**GK**TAL	--	--
AAA+ Domain PspF	2C98	Monomer	GERGT**GK**ELI	0.88	71
RuvB	1IN7	Monomer	GPPGT**GK**TTL	0.75	65
NSF-D2	1D2N	Hexamer	GPPHS**GK**TAL	0.95	47
SV40 Ltag Helicase	1SVL	Hexamer	GPIDS**GK**TTL	0.97	47
Bϕ12 ATPase P4	1W44	Hexamer	GKGNS**GK**TPL	1.08	48

Table 10: Superposition of the Rossmann fold (DI) in RuvBL1 with that of other AAA^{+} proteins. The PDB files were selected from recently published structures of AAA^{+} proteins. Rossmann folds from an arbitrarily chosen monomer in each PDB file were first superimposed using as a guide the last 6 residues in the listed Walker A region. A least-square fit between matching pairs of C^{α} atoms not more than 1.5 Å apart was then carried out.

The structure of RPA (Bochkarev et al. 1997) is composed of two domains with a similar fold, each formed by 7 β-strands. A ssDNA molecule is bound to this protein and makes contacts mainly through the phosphate backbone with both domains. The presumed DNA-binding region in RuvBL1 DII (residues 127-233) was superimposed with the N-terminal (residues 183-298) and C-terminal domains (residues 299-420) of RPA.

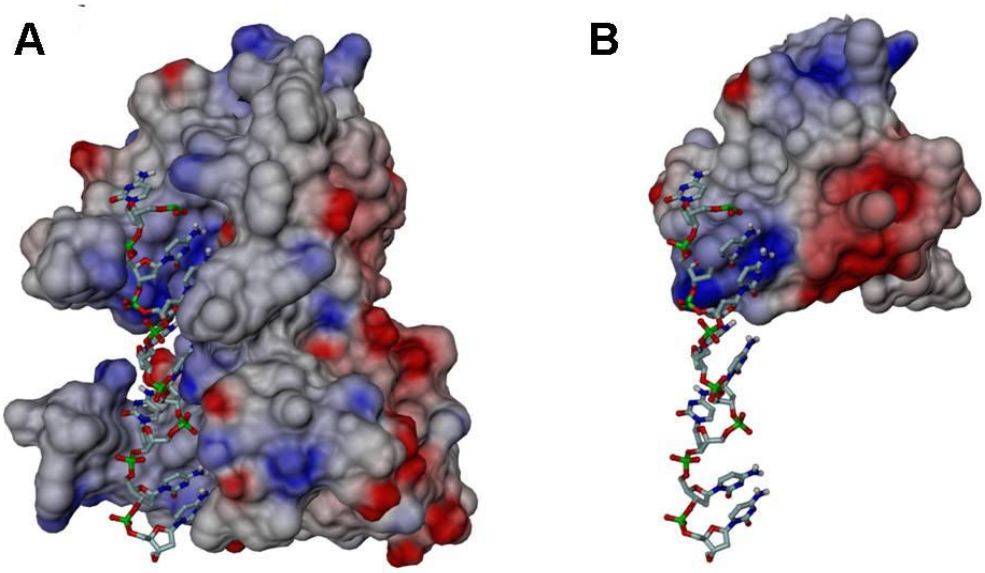

Figure 13: The DNA-binding region in RuvBL1 domain II. A, view of the electrostatic potential of the RPA molecule mapped at its molecular surface. The molecular surface was calculated with MSMS (Sanner et al. 1996) and the electrostatic potential was calculated with MEAD (Hubbard and Thornton 1993b). The range of potentials shows spans -5 (red, negative charge) to +5 kT/e (blue, positive charge) units. B, view of the electrostatic potential of the DNA binding region of RuvBL1 DII mapped at its molecular surface. As a visual aid, the ssDNA molecule bound to RPA is represented in ball-and-stick (Carbon, nitrogen, oxygen, and phosphorus atoms are coloured grey, blue, red, and green, respectively). Drawings were prepared with DINO (Philippsen 2002).

The surface charges in the DNA-binding region of RuvBL1 DII resemble those of the N-terminal domain (Figure 13A and B) in RPA. Nucleic acid-binding experiments confirmed that DII represents a new functional domain of eukaryotic AAA^+ motor proteins important for DNA/RNA binding (Figure 40). The smaller third domain, DIII, is all α-helical (α5−α9). One remarkable feature of DIII is that four helices (α5−α8) form a bundle located near the 'P-loop', important for ATP-binding, in which α5 and the beginning of α7 cover the ATP-binding pocket at the interface of DI and DIII (Figure 12B). This domain is similar to DII in RuvB (Figure 12B and C). The spatial arrangement of DI, DII and DIII in RuvBL1 could allow motions between domains.

4.1.4 Structure of the RuvBL1 hexamer

RuvBL1 assembles into a hexameric structure with a central channel (Figure 15A and B). In the crystal structure there are three independent monomers (A, B, and C) and two crystallographically non-equivalent hexamers (Figure 14). One hexamer is centered on a crystallographic 6-fold axis and is formed by the 6-fold repetition of monomer A, whereas the other is centered on a crystallographic 3-fold axis and is formed by the 3-fold repetition of monomers B and C (Figure 14).

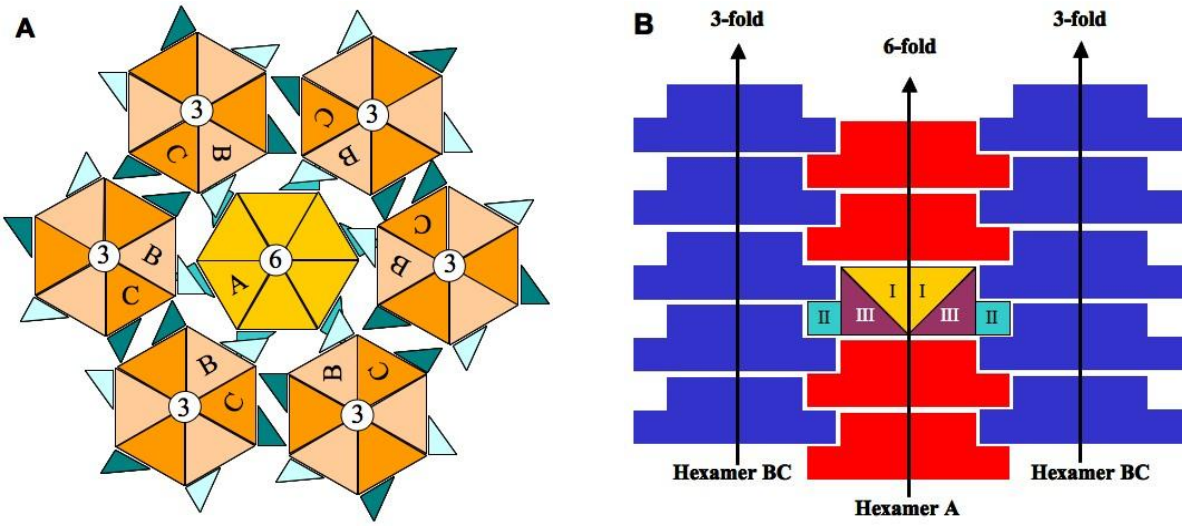

Figure 14: Scheme of RuvBL1 packing in the crystal. A, viewed from the top and B, viewed from the side: three independent monomers (A, B, and C) form two crystallographically non-equivalent hexamers. One consists only of monomers A and is centered on a crystallographic 6-fold axis. The other hexamer is centered on a crystallographic 3-fold axis and is formed by the 3-fold repetition of monomers B and C.

The three independent monomers have very similar three-dimensional structures. Superposition calculations between the three monomers by least-squares fit between pairs of C^{α} atoms not more than 1.5 Å apart give r.m.s. deviations between C^{α} atoms of 0.47 Å between monomers A and B, 0.58 Å between monomers A and C, and 0.43 Å between

monomers B and C. The total number of matched pairs C^{α} atoms is 300, 303, and 290, respectively, and these are mostly located in DI and DIII. Domain II has a similar fold but different orientations in monomers A and B and is highly disordered in monomer C. Viewed from the top (Figure 15B, with top and bottom as defined in Figure 15A), the external diameter of the hexameric ring ranges between 94 and 117 Å, and the central channel has an approximate diameter of 18 Å. Also its top surface (Figure 15A) appears to be remarkably flat. The hexamer bottom entrance is positively charged, whereas its inner surface and top entrance are negatively charged (Figure 16A and B), indicating a possible function in binding and translocating single-stranded nucleic acids. DII protrudes out of the hexameric ring (Figure 15).

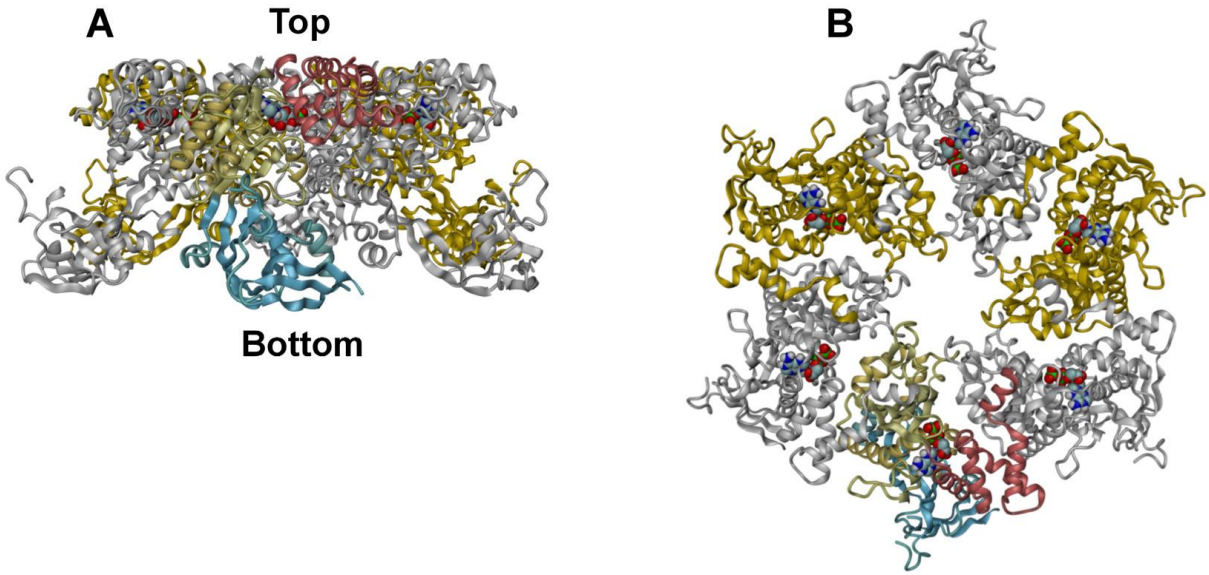

Figure 15: The RuvBL1 hexamer. A, ribbon diagram of the RuvBL1 hexamer (side view). Adjacent monomers are coloured light grey and gold. One gold monomer is coloured in the same way as in Figure 12B to highlight its domain structure. The hexamer herein represented is the crystallographic hexamer, formed by monomers A around the crystallographic 6-fold axis. The bound ADP molecules are depicted in space-filling mode, where each atom is represented by a sphere with a diameter twice its conventional van der Waals radius. Carbon, nitrogen, oxygen, and phosphorus atoms are coloured grey, blue, red, and green, respectively. B, ribbon diagram of the RuvBL1 hexamer (top view). The colouring scheme is as in A. Drawings were prepared with DINO (Philippsen 2002).

The connection between the nucleic acid-binding region of DII and the bulk of DI is achieved via a two-stranded extended β-region. This long connecting region probably allows DII some freedom of motion in relation to DI and DIII. Indeed, since in the RuvBL1 hexamer there are no direct contacts between domain II and either DI or DIII, it is very likely that the conformation and position of DII in the crystal structure was determined by crystal packing. DII of hexamer A packs between domains I and III of molecule B in hexamer BC. DII in molecule B packs against domains I and III of molecule A. However, DII in molecule C has

no close crystal contacts, and this probably explains why it could not be fully seen in the electron density maps. A further indication of molecular disorder is given by the values of the average thermal motion parameter B listed in Table 9; they are lowest for monomer A and highest for monomer C, consistent with the increasing number of residues (see above) that could not be seen in the electron density and thus were not included in the structural model. On the other hand, the B-values for the ADP ligand atoms are consistently similar to those of the protein atoms in the binding pocket. The interface between adjacent subunits in the RuvBL1 hexamer is made up entirely by DI and DIII and exhibits a well defined shape complementarity. As shown in Figure 16C, the hexamerisation in the structure of the RuvBL1·ADP complex blocks the nucleotide binding pocket, thus making an exchange from ADP to ATP impossible. This may explain the inability to co-crystallize the non-hydrolysable ATP analog AMP-PNP into this crystal form because this compound would require an open conformation of the active site.

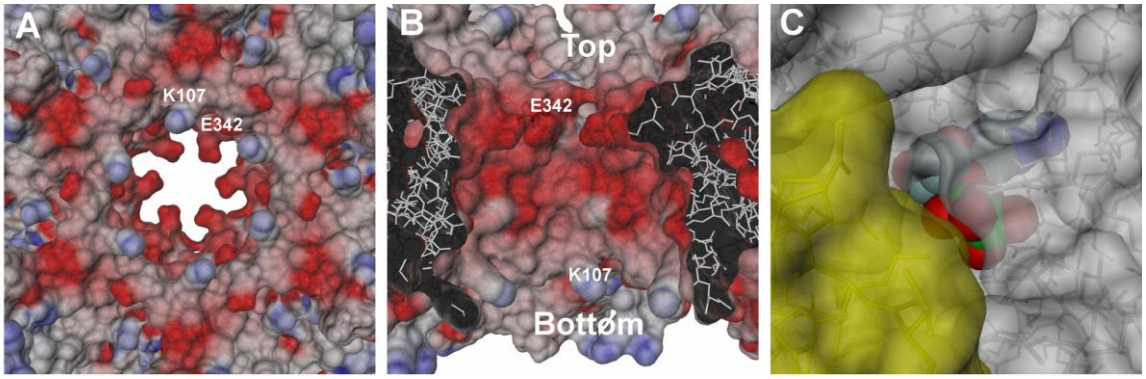

Figure 16: The central channel of the RuvBL1 hexamer. A and B, views of the electrostatic potential mapped at the molecular surface. The molecular surface and the electrostatic potentials were calculated as in Figure 13 for the whole hexamer. The range of potentials shows spans -5 (red, negative charge) to +5 kT/e (blue, positive charge) units. The labelled residues (Lys107 and Glu342) are the most conspicuous positively and negatively charged residues. Lys107 is located near the channel bottom and Glu342 near its top. In A the hexamer is shown in bottom view (as defined in Figure 15A). In B a cross-section view of the central channel (same orientation as in Figure 15A) is represented, showing a negatively charged patch that covers most of its surface. C, view of the interface between adjacent monomers in the RuvBL1 hexamer, showing blocking of the nucleotide-binding pocket upon hexamer formation. The molecular surfaces represented (gold and white) were calculated as in Figure 13A and B. The ADP molecule is represented in space-filling mode, as in Figure 12B.

4.1.5 Motifs for ATP Binding and Hydrolysis

Structural analysis and sequence conservation identify four motifs at the DI-DIII boundary (Walker A, Walker B, sensor 1 from DI, and sensor 2 from DIII; Figure 12A and Figure 17A) likely to be important in nucleotide-driven conformational changes of the protein structure. The Walker A motif, also termed the P-loop, is important for ATP binding. It coordinates the triphosphates and positions the γ-phosphate group for cleavage. The Walker A residues Gly70

to Leu79 in RuvBL1 have corresponding conserved residues in all structures listed in Table 14, the similarity being higher with bacterial RuvB and NSF-D2. Using the superimposed coordinates of RuvBL1, RuvB (Putnam et al. 2001), NSF-D2 (Lenzen et al. 1998), and SV40 large tumour antigen helicase (Gai et al. 2004; Li et al. 2003) together with the AMP-PNP and Mg^{2+} ligands in NSF-D2, an ATP bound to RuvBL1 was modelled. The nucleotide-binding pocket in RuvBL1 is sufficiently large to accommodate an ATP molecule, and the γ-phosphate will occupy a volume that contains three water molecules in the ADP-bound structure (Figure 17). Furthermore, based on the observed coordination of Mg^{2+} in NSF-D2 and SV40 large tumour antigen helicase, it is reasonable to assume that this cation could bind in an equivalent position in RuvBL1·ATP. Within the Walker A motif, Gly73 could stabilise the γ-phosphate by interacting with one of its oxygens, and Thr77 could be involved in coordinating the Mg^{2+} (Figure 17B).

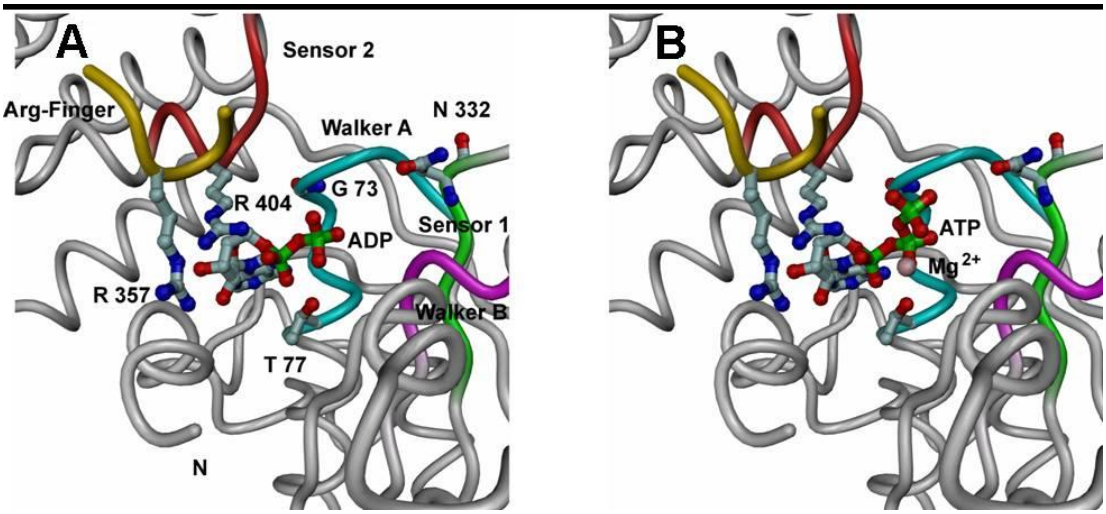

Figure 17: Nucleotide-binding pocket of RuvBL1. A, Tube view of RuvBL1 in the vicinity of the nucleotide binding pocket, showing the Walker A (cyan), Walker B (violet), sensor 1 (green) and sensor 2 (red) regions as well as the Arg finger region from the adjacent monomer (gold). The ADP molecule and the side chains of important residues are represented in ball-and-stick mode. Carbon, nitrogen, oxygen, and phosphorus atoms are coloured grey, blue, red, and green, respectively. B, a similar view as in A, showing the modelled positions of ATP and Mg^{2+}.

The Walker B motif residues Asp302-His305 are responsible for ATP hydrolysis. They lie at an adequate position to interact with Mg^{2+} and likely activate the water nucleophile for ATP cleavage. In addition to the Walker motifs, Asn332 in sensor 1, located in DI between the Walker A and B motifs, and Arg404 in sensor 2 make polar interactions with the β- or γ-phosphate groups. The function of sensor 1 is to distinguish between nucleotide diphosphate and triphosphate states by forming a hydrogen bond with the ATP γ-phosphate group. Based on the ATP-bound model, a simple rotamer change in response to ATP binding could bring either oxygen or nitrogen from the side chain of Asn332 into a suitable position for hydrogen

bond formation with the terminal oxygen from γ-phosphate, without a significant backbone conformational change.

The loop linking helix α6 to helix α7 protruding from DIII contains the sensor 2, which is characterised by a highly conserved Arg residue (Neuwald et al. 1999). It packs against the nucleotide-binding site and distinguishes between nucleotide-bound and unbound states. Arg404 in sensor 2 interacts with components of the nucleotide present in both ADP and ATP.

The conserved Arg357 corresponds to Arg170 in RuvB, which was shown to function as an Arg finger (Putnam et al. 2001), allowing the efficient hydrolysis of ATP by binding to the γ-phosphate group. In the RuvBL1 hexamer, Arg357 from the adjacent monomer contributes to the active site and is in sufficiently close proximity to the nucleotide-binding pocket to be able to act as an Arg finger, provided a suitable conformational change takes place. This arrangement of active-site residues suggests some degree of cooperativity between monomers. Therefore, I propose that hexamerisation is critical for ATP hydrolysis in RuvBL1. Monomer assembly into hexamers is known to be crucial for the function of other AAA^+-class ATPases (Neuwald et al. 1999).

4.2 Attempts to obtain the crystal structure of RuvBL2

4.2.1 Purification of RuvBL2

RuvBL2 was purified in the same way as RuvBL1 using affinity and anion exchange chromatography (see chapter 4.1.1). The SDS-PAGE monitoring the purification is shown in Figure 18. Purified RuvBL2 was used for crystallization and functional studies. In addition analytical gel filtration experiments were performed using the purified protein. These experiments showed that RuvBL2, which has a molecular weight of 53 kDa, was a monomer at lower concentrations (~1.5 mg/ml), but formed a high molecular weight oligomer following concentration above 3 mg/ml or addition of ATP. In contrast monomeric RuvBL1 exhibited no oligomerisation after ATP addition. Figure 19 shows the oligomerisation of RuvBL2 after addition of 2 mM ATP.

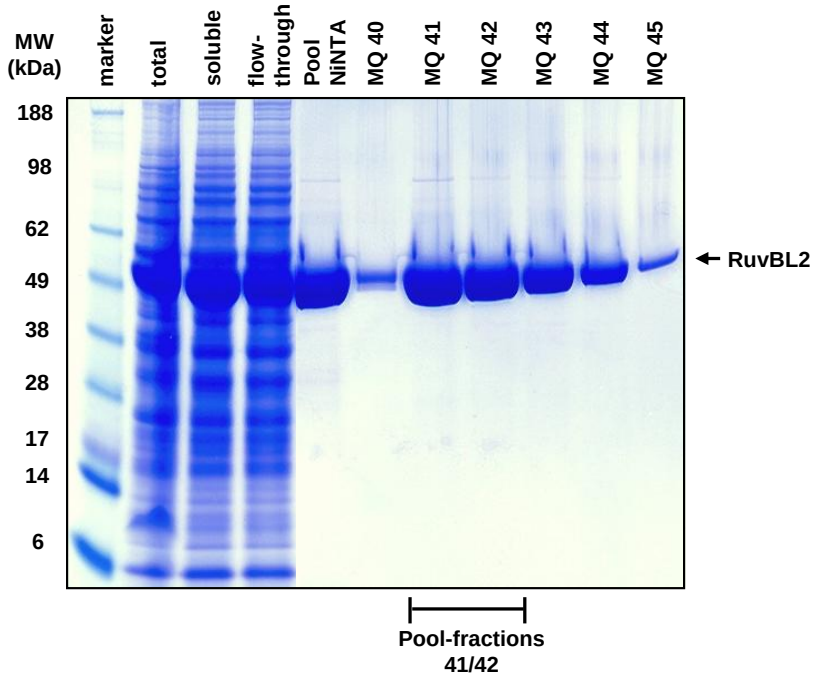

Figure 18: SDS-PAGE monitoring the purification of RuvBL2. Following cell disruption (total) the soluble proteins were loaded onto a Ni-NTA column. The pool of RuvBL2 containing fractions was the input (Pool Ni-NTA) for the second purification step (MonoQ). Main fractions MQ41 and 42 of the RuvBL2 peak were used for crystallization and functional studies.

The chromatograms of the analytical gel filtration experiments (Figure 19) show peaks at 1.44 ml and 1.19 ml corresponding to an apparent molecular weight of 80 kDa and 620 kDa, respectively. Since the molecular weight of the RuvBL2 monomer is 53 kDa, the peak at 620 kDa is compatible with a dodecameric structure. However, a distinction between the hexameric and dodecameric state of RuvBL2 using a Superdex 200 column was not reliable, because this column does not allow separation in the high molecular weight range above 200 kDa (see protein standard in Figure 19C). DLS experiments confirmed the results of analytical gel filtration. RuvBL2 was a monomer exhibiting an apparent molecular weight of 73 kDa at 1 mg/ml and formed a hexamer (262 kDa) at the same concentration after adding 2 mM ATP. Small-angle x-ray scattering experiments (see chapter 4.4) showed that RuvBL2 formed hexameric and dodecameric structures at concentrations above 3 mg/ml.

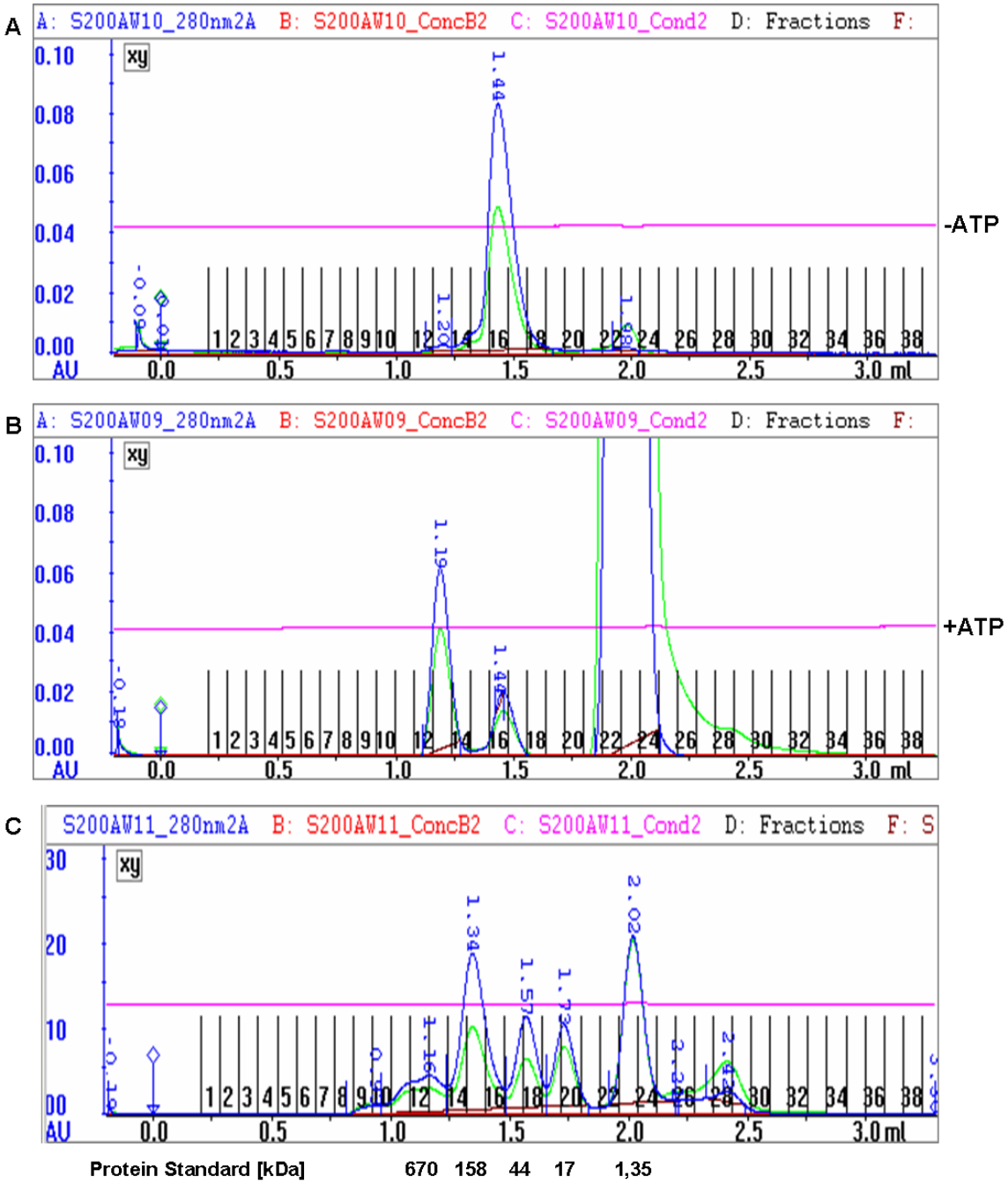

Figure 19: Analytical gel filtration of RuvBL2. A, RuvBL2 is a monomer at 1.5 mg/ml, but forms a high molecular weight oligomer after addition of 2 mM ATP (B). C, chromatogram of the protein standard in order to calculate the molecular masses of the RuvBL2 samples shown in A and B.

4.2.2 Crystallization of RuvBL2

Prior to screening for crystallization conditions RuvBL2 was concentrated to 20 mg/ml. The best hits for crystallization of wild-type RuvBL2 were E12 (1.6 M ammonium sulphate, 0.1 M Bicine pH 9) and G7 (1.5 M ammonium sulphate, 0.1 M Tris-HCl pH 8.5; 11.9 % (v/v) glycerol anhydrous) of the AmSO4 screen (QIAGEN). These conditions were optimised in

24-well plates by performing a pH gradient from 7 to 9. The best crystals were obtained using a solution containing 1.5 M ammonium sulphate and 0.1 M Bicine pH 8 at 293 K (Figure 20). The crystals were tetragonal bipyramidal, appeared after one day and grew within five days to a size of approximately 300 x 280 µm. However, these crystals did not diffract and could not be improved by additives or co-crystallization with ADP, ATP or the non-hydrolysable ATP analog AMP-PNP. The search for completely new conditions was not successful either.

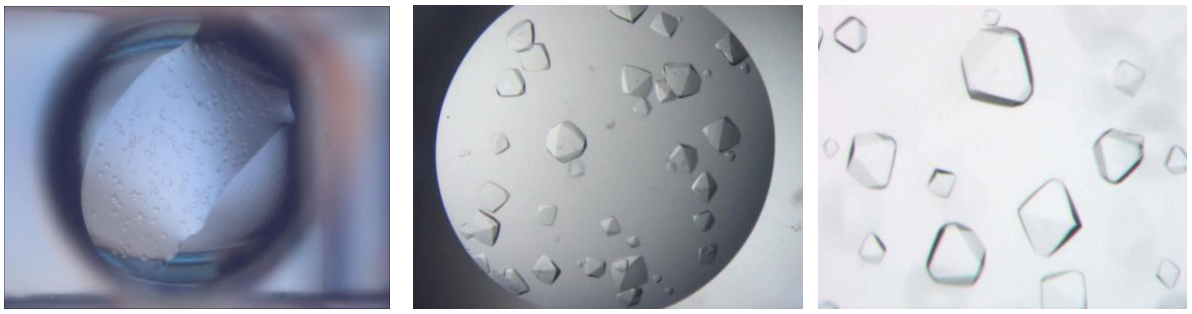

A) G7 of AmSO4 Screen B) reproduced 24-well drop C) optimised crystals

Figure 20: RuvBL2 crystals. A, G7 drop of the 96-well plate (AmSO4 Screen). B, 24-well plate drop showing reproduced crystals. C, optimised crystals that were obtained by performing a pH gradient.

Since diffraction requires highly ordered molecules in all three dimensions, crystals with an internal disorder give no diffraction pattern. There are several possible reasons explaining why crystals do not diffract. In most cases the internal order of the crystal is limited due to flexible regions present within the protein molecule or to bulky charged residues on the protein surface. In order to obtain diffracting crystals, 21 mutants of RuvBL2 were cloned (Table 11). First a model of the RuvBL2 structure based on the RuvBL1 structure was built using the program MODELLER (Eswar et al. 2000). Bulky charged residues on the molecular surface of RuvBL2, like glutamic acid and lysine clusters were replaced by alanine creating 11 surface mutants of RuvBL2 (#1-11 in Table 11). In addition the structure of RuvBL1 shows that DII is very flexible. In the RuvBL1 structure DII is stabilised by crystal packing (see chapter 4.1.4), but in the homolog RuvBL2 the large flexible domain might disturb the order of the crystal. Diverse DII deletion constructs were therefore cloned in order to truncate this large flexible domain (#12-17 in Table 11). In one mutant the whole domain II was excised from RuvBL2, but the resulting construct was not soluble suggesting that domain II is at least in part essential for protein solubility. Two amino acid residues of domain II in the RuvBL1 structure make crystal contacts. In order to obtain the same crystal contacts in RuvBL2 the corresponding residues were mutated (I138Y and A198N). Furthermore the C- and N-termini of RuvBL2 were truncated, because both termini are longer than in RuvBL1

(#19-21 in Table 11). Table 11 lists all mutants and summarises whether the constructs were soluble and whether purification and crystallization were successful.

Number	Mutant	Solubility	Purification/Concentration	Crystallization
1	R2_**KEE**132	yes	yes	no
2	R2_**E**I**Q**144	yes	yes	no
3	R2_**E**I**Q**ID**R**144	no	—	—
4	R2_**K**VG**K**157	yes	no	—
5	R2_**E**M**E**167	yes	yes	no
6	R2_**E**SLT**K**D**K180**	no	—	—
7	R2_**K**S**E**269	yes	yes	no
8	R2_**EK**364	yes	no	—
9	R2_**D**V**E**379	yes	no	—
10	R2_**RK**416	yes	no	—
11	R2_**KE**444	yes	no	—
12	R2-DII_K132-V239	yes	yes	no
13	**R2-DII_E133-V238**	**yes**	**yes**	**yes**
14	R2-DII_N251-AAA-I276	no	—	—
15	R2-DII_N251-4xA-I276	no	—	—
16	R2-DII_N251-AAA-I276A	no	—	—
17	R2-DII_N251-4xA-I276A	no	—	—
18	R2_I138Y_A198N	yes	yes	no
19	R2-N terminus	yes	yes	no
20	R2-C terminus	yes	yes	no
21	R2-N & C termini	yes	yes	no

Table 11: RuvBL2 mutants. Summary showing the results of solubility tests and the success of purification and crystallization.

Only one mutant could be crystallized, namely RuvBL2-DII (R2-DII, #13 in Table 11). In this construct the domain II consisting of 170 amino acids was 105 amino acids shorter, because the residues between Glu133 and Val238 were excised and replaced by the small linker GPPG. The Nuclear Receptor Screen (Molecular Dimensions) contained the best hits for crystallization conditions (Figure 21A and B): C11 (1.1 M sodium tartrate, 0.2 M ammonium sulphate, Tris pH 8), D11 (1.1 M sodium tartrate, 0.1 M magnesium chloride, HEPES pH 7.5) and G10 (0.8 M sodium tartrate, 0.3 M ammonium acetate, HEPES pH 7.5).

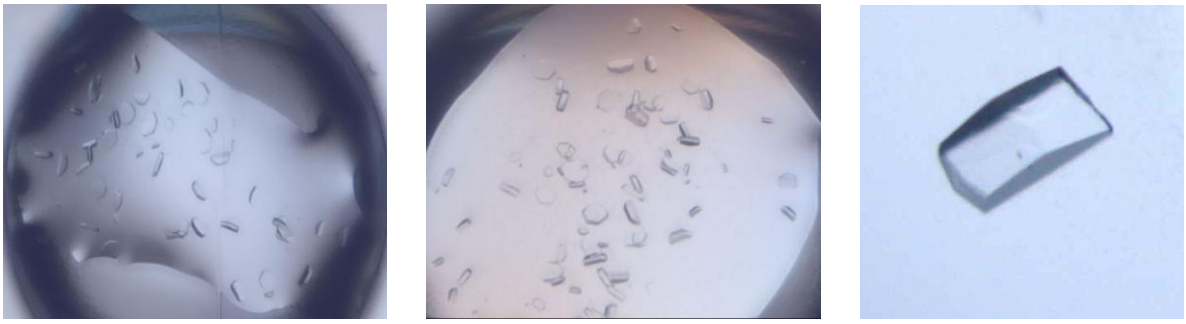

A) D11 of Nuclear Receptor Screen B) G10 of Nuclear Receptor Screen C) optimised crystal

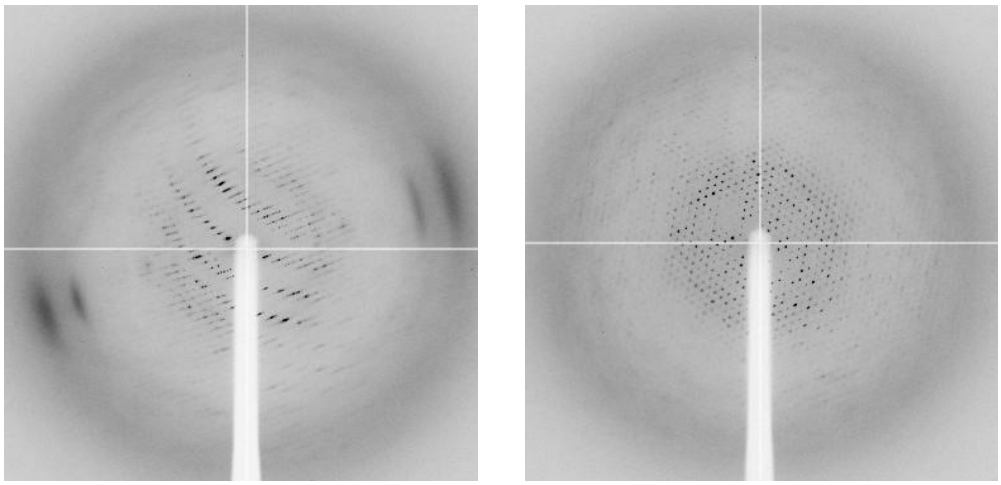

D) diffraction pattern of RuvBL2-DII

Figure 21: Crystals and diffraction images of RuvBL2-DII.

The crystals were reproduced and optimised in 24-well plates. They were tested at the European Synchrotron Radiation Facility (ESRF) in Grenoble and diffracted to 2.9 Å. Due to the high mosaicity of the crystals, the collected datasets could not be used for structure determination (Figure 21D). Mosaicity is the deviation from an ideally ordered crystal and emerges from disorder in the crystal giving rise to reflections over a certain angular range. It can be used as an indicator of crystal perfection. A spatial separation of some reflections in the diffraction pattern was not possible owing to a long c-axis of the unit cell and the high mosaicity.

In order to improve the crystals a screening for optimised buffer conditions was performed using the thermal shift assay. It was shown that the imidazole from buffer B during the first affinity chromatography caused protein precipitation. For that reason a buffer exchange using a desalting column (HiPrep^{TM} 26/10, Amersham) was necessary. In addition 5 mM ADP were added to the protein before crystallization, because thermal shift assay results indicated a stabilisation of R2-DII. Although the crystallization conditions of the slightly different purified RuvBL2-DII construct differed from the initial conditions (0.7 M trisodium citrate,

0.1 M HEPES pH 7.4) and the hexagonal crystals became thicker (Figure 21C), the problems concerning mosaicity and a long c-axis persisted. A possible way to improve the mosaicity may be a different way of freezing the crystals, although several cryo-conditions have been tested already.

4.3 Purification and crystallization of the RuvBL1/RuvBL2 complex

4.3.1 Purification of the RuvBL1/RuvBL2 wild-type complex

The RuvBL1/RuvBL2 complex (R1/R2) was purified in three steps as indicated in Figure 22 using two affinity purifications and a gel filtration. An important prerequisite for the complex purification were the different tags in RuvBL1 and RuvBL2, which were expressed with a 6xHis and a FLAG tag, respectively.

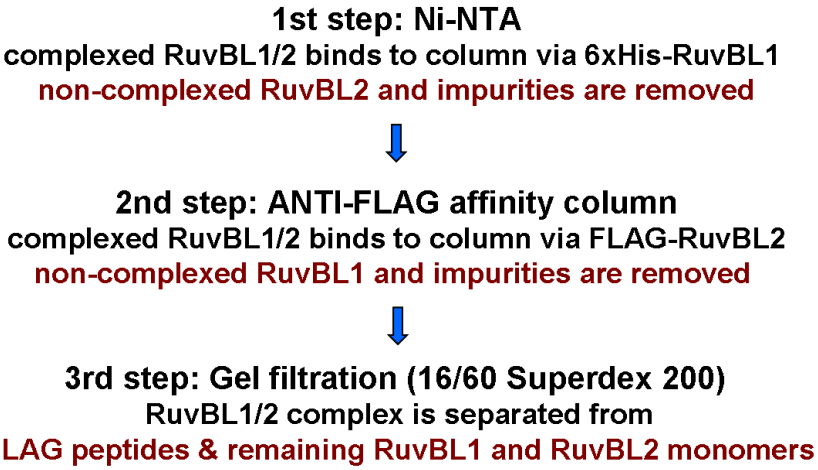

Figure 22: Purification scheme of the RuvBL1/RuvBL2 complex. The first affinity purification step retained 6xHis tagged RuvBL1 and associated proteins using the Ni-NTA affinity column. Non-complexed RuvBL2 and main impurities were left in the flow-through. In the second purification step the ANTI-FLAG affinity column pulled the FLAG tagged RuvBL2 in the R1/R2 complex removing non-complexed RuvBL1 that bound to the first column. A gel filtration column separated the R1/R2 complex from remaining monomers and from the FLAG peptides that were used for elution in the second purification step.

After co-expression of 6xHis-RuvBL1 and FLAG-RuvBL2 the soluble proteins were loaded onto a Ni-NTA Superflow (QIAGEN) column in the presence of 20 mM imidazole. The Ni-NTA column retained the 6xHis tagged RuvBL1 and associated proteins after removing unspecific bound proteins by washing. RuvBL1 and the RuvBL1/RuvBL2 complex eluted in a gradient between 80 and 240 mM imidazole (Figure 23A). Analysing all peak fractions using an SDS-PAGE (Figure 23B) revealed that the eluted protein was not pure at this stage.

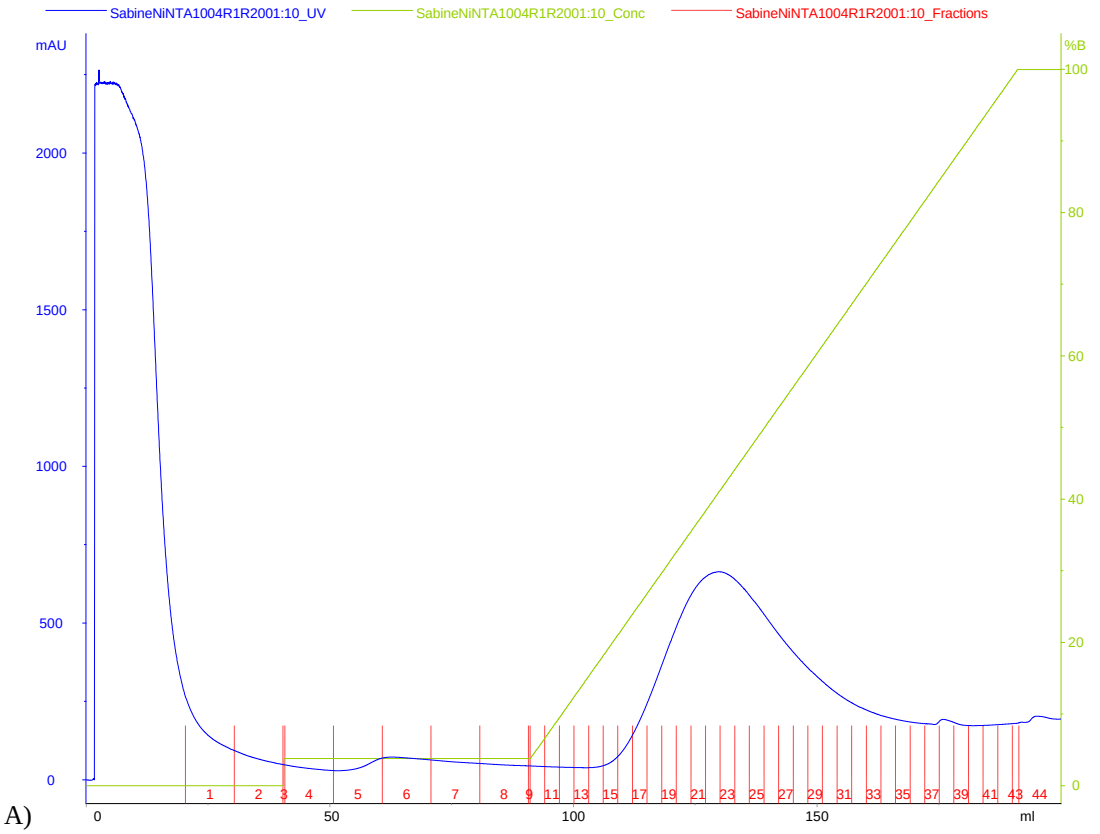

A)

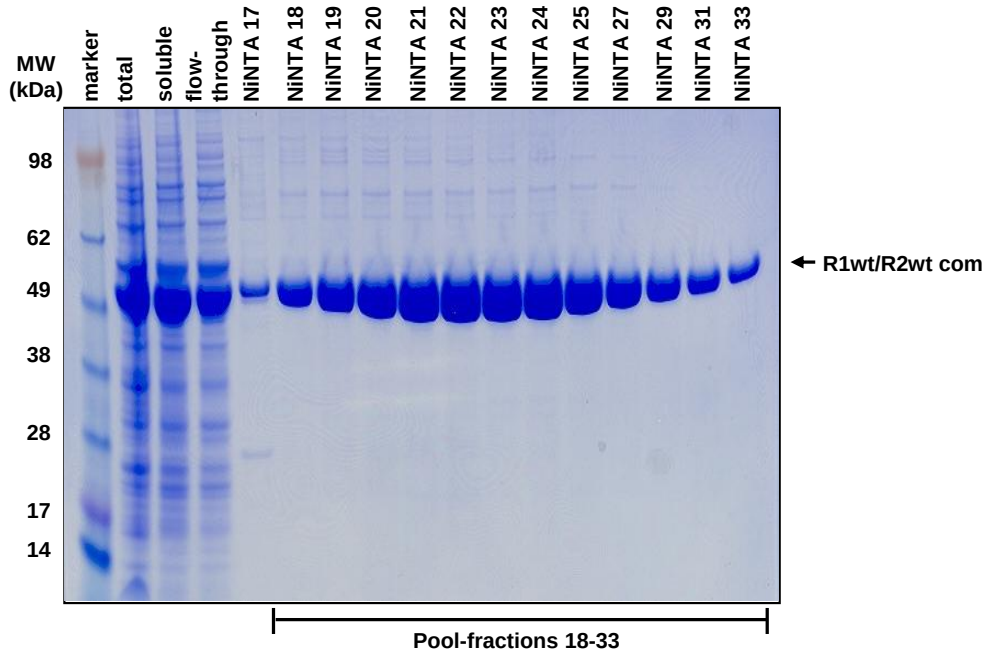

B)

Figure 23: First step of the RuvBL1/RuvBL2 complex purification. A, Ni-NTA chromatography profile. The 6xHis tagged RuvBL1 and associated proteins eluted in the gradient between 80 and 240 mM imidazole (blue peak). The green curve indicates the percentage of buffer B, whereas the blue curve shows the protein absorption at 280 nm. B, SDS-PAGE analysis of the peak fractions.

In order to remove non-complexed RuvBL1 and impurities the Ni-NTA peak fractions 18-33 were pooled and loaded onto an Anti-FLAG affinity column (SIGMA). Binding to that column is based on antigen-antibody interactions and therefore highly specific. Only FLAG

tagged RuvBL2 could bind to the column. The RuvBL1/RuvBL2 complex was eluted using 2 column volumes of FLAG peptides (Figure 24A).

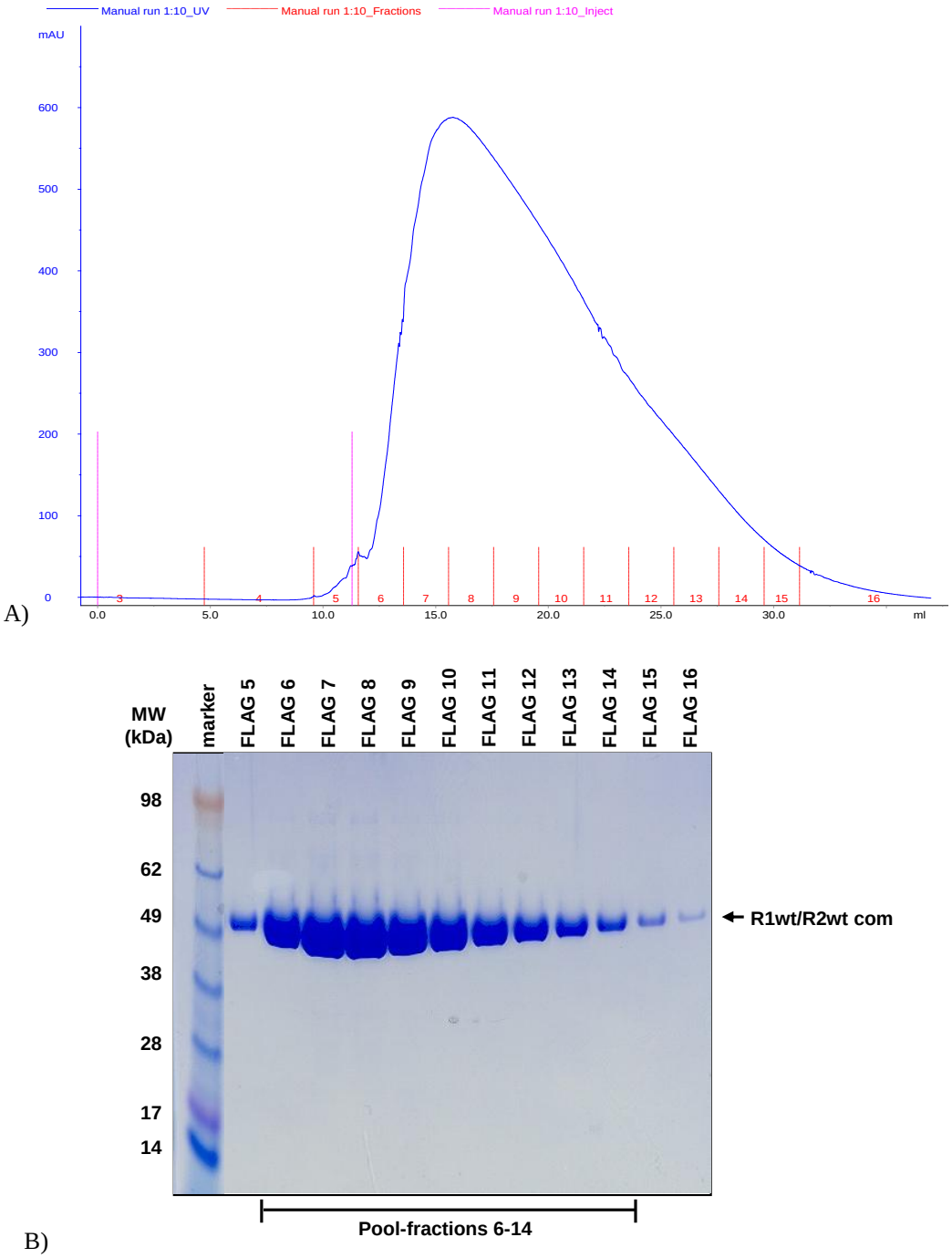

Figure 24: Second step of the RuvBL1/RuvBL2 complex purification. A, Anti-FLAG chromatography profile. The FLAG tagged RuvBL2 and associated RuvBL1 eluted after addition of FLAG peptides (pink mark). The blue curve shows the protein absorption at 280 nm. B, SDS-PAGE analysis of the peak fractions.

SDS-PAGE analysis (Figure 23B) showed that the eluted proteins were pure at this stage. In order to obtain a uniform purified RuvBL1/RuvBL2 complex and remove the FLAG peptides, a size exclusion chromatography was performed as last purification step. The Anti-FLAG

affinity pool consisting of fractions 6-14 was loaded onto the HiLoad™ 16/60 Superdex 200 (Amersham Biosciences) column (Figure 25).

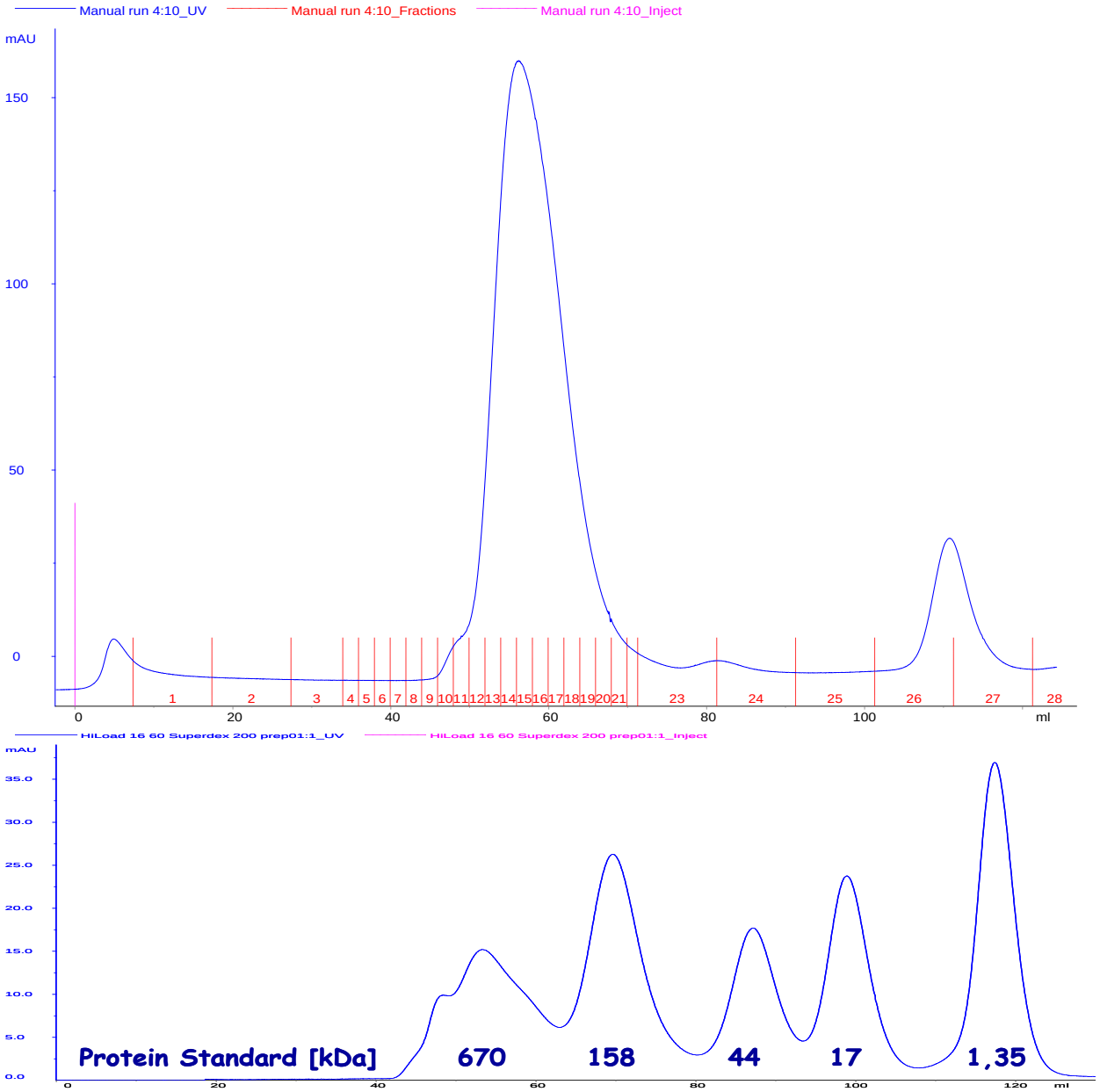

Figure 25: Gel filtration of the RuvBL1/RuvBL2 complex. The protein standard indicates the positions, where proteins with a given molecular weight elute. The R1/R2 complex (upper chromatogram) eluted at a position with an apparent molecular weight of 550 kDa that corresponding to a dodecamer. The small peak that appears at 110 ml corresponds to the FLAG peptides.

The RuvBL1/RuvBL2 complex eluted at a position of 550 kDa corresponding to a dodecamer. RuvBL1 and RuvBL2 have a molecular weight of 52 and 53 kDa, respectively. A dodecamer consisting of RuvBL1 and RuvBL2 in a 1:1 molar ratio would have a molecular weight of 630 kDa. Since in gel filtration molecules are separated according to differences in their globular size, the molecular weight estimated from the protein standard is not accurate. It is possible that the huge peak contained a mixture of RuvBL1/RuvBL2 hexamers and

dodecamers, because the Superdex 200 column is not applicable for separation purposes for a high molecular weight range above 200 kDa. In addition the chromatogram shows a small peak at 50 kDa corresponding to monomers. The separated FLAG peptides eluted at a position of 1.5 kDa. Gel filtration results demonstrate that the large RuvBL1/RuvBL2 complex was separated from remaining monomers and from the FLAG peptides that were used for elution in the second purification step (Figure 25). The complex was highly pure after the third purification step (Figure 26A). Owing to the similar molecular weight of RuvBL1 and RuvBL2 both proteins ran at the same height in a standard SDS-PAGE (Figure 26A). For that reason a very sensitive automated SDS-PAGE (Caliper) was used to determine the molar ratio of RuvBL1 and RuvBL2 within the complex. The results show that RuvBL1 and RuvBL2 were present in the complex in a 1:1 molar ratio (Figure 26B). Analytical Western Blots confirmed these results (data not shown).

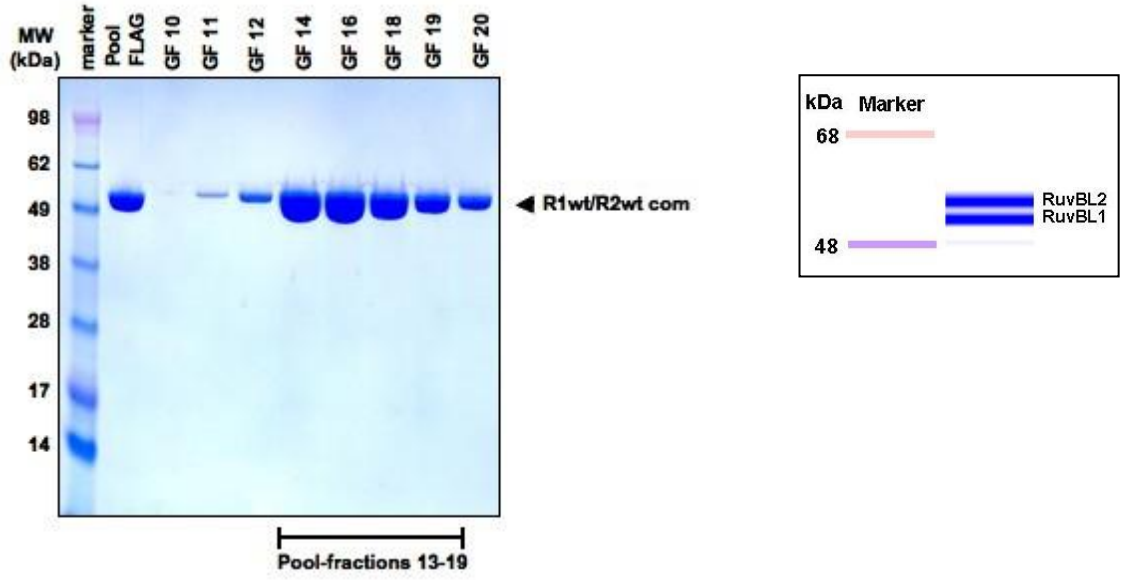

A) B)

Figure 26: SDS-PAGE analysis of the RuvBL1/RuvBL2 complex. A, standard SDS-PAGE. B, automated electrophoresis system separating the RuvBL1 and RuvBL2 bands.

The gel filtration peak pool consisting of fractions 13-19 was concentrated to diverse final concentrations (10–40 mg/ml) and used for crystallization trials. Although thousands of conditions were tested, the wild-type complex never crystallized. Crystallization of the complex might be disturbed by 12 flexible domains II in the RuvBL1/RuvBL2 structure. For that reason deletion mutants of RuvBL1 and RuvBL2 with truncated domains II were cloned and characterised.

4.3.2 Characterisation of mutated RuvBL1/RuvBL2 complexes

In order to co-express and purify truncated versions of the complex, the regions necessary for interaction between RuvBL1 and RuvBL2 needed to be verified first. It was assumed that the flat surface of the RuvBL1 hexamer (Figure 15A) represented a possible interaction site between two hexamers for the formation of a dodecamer. Since domain I and domain III in RuvBL1 are needed to form the hexameric ring, only domain II which protrudes out of the hexameric ring was truncated in RuvBL1 and RuvBL2. In RuvBL1 the part between Glu126 and Ile234 was deleted and replaced by the amino acid linker GPPG, whereas in RuvBL2 the corresponding region between Glu133 and Val238 was cut out and replaced by the residues GPPG. Hence domain II, which consists of about 175 amino acids in the natural proteins, lacked 107 residues in the RuvBL1 deletion mutant and 104 residues in the RuvBL2 deletion mutant. In addition, the part of RuvBL2 domain II that was truncated in the deletion constructs was co-expressed with wild-type RuvBL1 and RuvBL1-DII, in order to test whether this cut-out part was involved in interaction between RuvBL1 and RuvBL2. The following constructs were used for co-expression and interaction studies:

6xHis-RuvBL1wt + FLAG-RuvBL2-DII

6xHis-RuvBL1wt + FLAG-DII of RuvBL2 (partial DII)

6xHis-RuvBL1-DII + FLAG-RuvBL2-DII

6xHis-RuvBL1-DII + FLAG-DII of RuvBL2 (partial DII)

Following transformation of *E. coli* and induction of expression, cell lysates were obtained and cleared. They were then loaded onto a small Ni-NTA affinity column which bound to the 6xHis tag of the RuvBL1 constructs. After washing the column several times the bound proteins were eluted with buffer containing 400 mM imidazole (see buffer B in 3.3). Only RuvBL2 constructs associated with 6xHis-RuvBL1 were eluted. The elution pool was loaded onto a SDS-PAGE (Figure 27A) and verified using Western Blot (shown exemplarily for the RuvBL1-DII/RuvBL2-DII complex in Figure 27B).

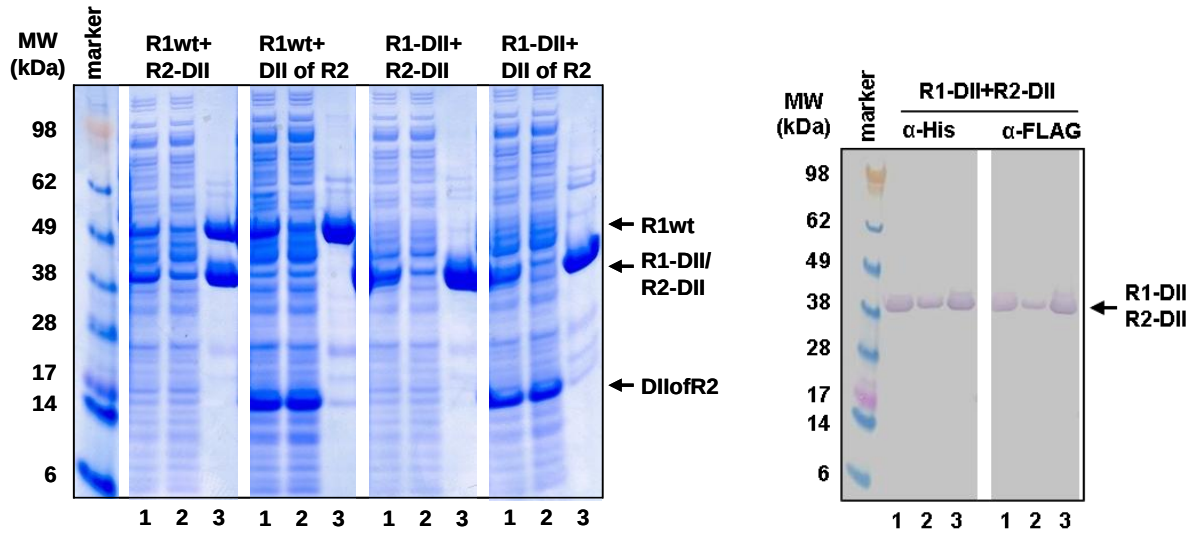

A) SDS-PAGE of deletion mutants

B) Western Blot of R1-DII+R2-DII

Figure 27: Interaction between deletion constructs of RuvBL1 and RuvBL2. A, SDS-PAGE showing proteins that eluted from the Ni-NTA, 1 = total, 2 = cleared lysate, 3 = Ni-NTA elution pool. B, Western Blot detection of RuvBL1 and RuvBL2 deletion constructs in the complex. Equal amounts of proteins were separated by SDS-PAGE and subsequently transferred to a polyvinylidene fluoride membrane. Immunodetection was performed with anti-His and anti-FLAG antibodies to detect RuvBL1 and RuvBL2, respectively.

RuvBL1 in the 6xHis-RuvBL1/FLAG-RuvBL2-DII co-expression sample bound to the Ni-NTA and also FLAG-RuvBL2-DII was eluted. Both proteins were present at a 1:1 molar ratio (Figure 27A, R1wt+R2-DII lane 3). In contrast, the part of domain II (E134-E237) that was truncated in RuvBL2-DII and co-expressed with RuvBL1wt was not eluted from the column (Figure 27A, R1wt+DII of R2, lane 3). This result indicates that the truncated part of domain II did not interact or was not sufficient for a stable interaction with wild-type RuvBL1. Interestingly, RuvBL1-DII and RuvBL2-DII, which both have a truncated domain II, were eluted together and remained associated (Figure 27A, R1-DII+R2-DII, lane 3) suggesting that both truncated proteins can stably interact. For that reason the missing residues T127-E233 in domain II of RuvBL1 and E134-E237 in domain II of RuvBL2 were not essential to form a stable RuvBL1/RuvBL2 complex. Because of the similar molecular weights of RuvBL1-DII and RuvBL2-DII (41 and 42 kDa, respectively) both proteins were not distinguishable after the SDS-PAGE (Figure 27A, R1-DII+R2-DII, lane 3). However, Western Blot analysis using anti-His and anti-FLAG antibodies confirmed that RuvBL1-DII and RuvBL2-DII were present in the complex (Figure 27B). The partial DII of RuvBL2 (E134-E237) did not interact with RuvBL1-DII, because only RuvBL1-DII was eluted from the Ni-NTA column (Figure 27A, R1-DII+DII of R2, lane 3) suggesting that the partial domain II cannot associate with the truncated RuvBL1. From these data it can be inferred that either the flat surface composed

of DI and DIII or the remaining part of DII still present in the deletion constructs was important for interaction between two hexamers to form a dodecameric structure. The constructs able to form a complex, namely RuvBL1wt/RuvBL2-DII and RuvBL1-DII/RuvBL2-DII, were purified and used for further investigations.

4.3.3 Purification and crystallization of RuvBL1/RuvBL2 complexes with truncated domains II

The complexes formed of RuvBL1 and RuvBL2 containing truncated domains II were purified in the same way as the wild-type complexes (Figure 22). In gel filtration, the RuvBL1wt/RuvBL2-DII and RuvBL1-DII/RuvBL2-DII complexes eluted at the position of a high molecular weight oligomer similarly to the wild-type complex, suggesting that truncation of DII did not interfere with oligomerisation. Figure 28 demonstrates the increase of purity during the process of complex purification.

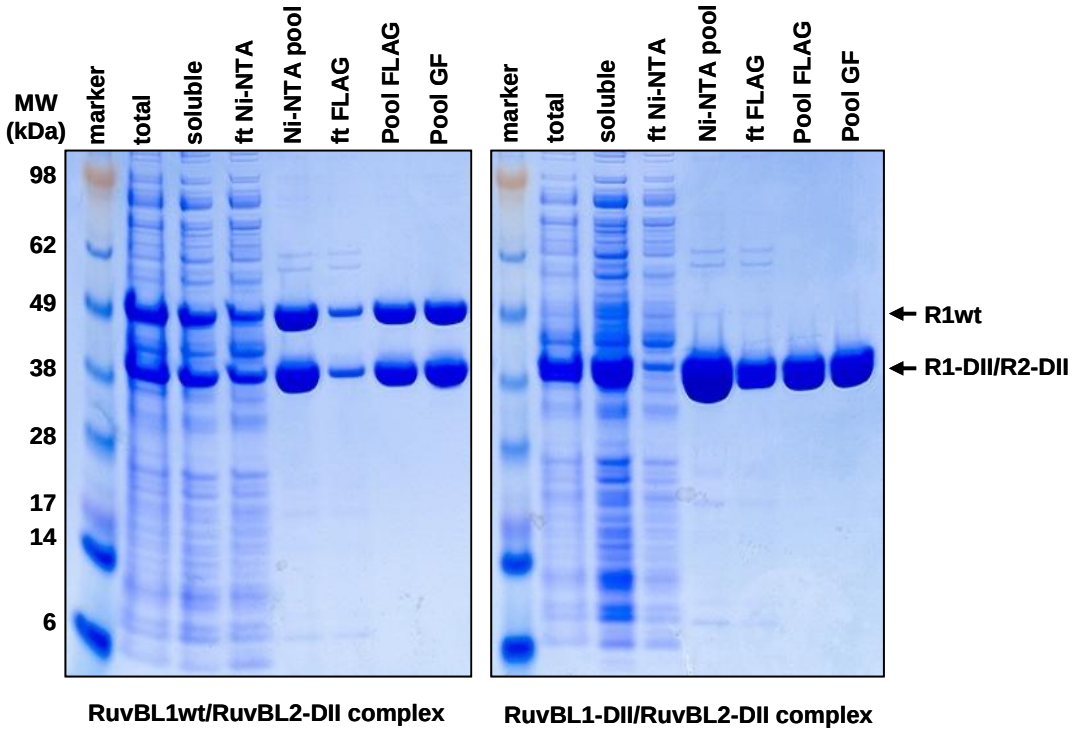

Figure 28: SDS-PAGE of R1wt/R2-DII and R1-DII/R2-DII complex purification. Following cell disruption (total, 1µl) the soluble proteins were loaded onto a Ni-NTA column. In the second purification step (Anti-FLAG affinity column) all impurities of the Ni-NTA pool (10 µl) were found in the flowthrough (ft FLAG, 10 µl) and a pure complex was obtained (Pool FLAG, 10 µl). To remove the FLAG peptides and remaining monomers a gel filtration constituted the last purification step (Pool GF).

The purified complexes were concentrated to 20 mg/ml and used for crystallization trials. In contrast to the wild-type complex, the deletion complexes formed crystals. When searching for initial crystallization conditions of RuvBL1wt/RuvBL2-DII, the best hits were found in

the PEG Screen (QIAGEN) namely E2, E4, E8 and F2 which all contained 20 % PEG 3350 and different additives. In addition the JSCG Screen (QIAGEN) contained hits at B4 (0.1 M HEPES pH 7.5, 10 % PEG 8000, 8 % ethylene glycol), C4 (0.1 M HEPES pH 7, 10 % PEG 6000) and G7 (15 % PEG 3350, 0.1 M succinic acid). The results were reproduced and optimised at the microliter scale using sitting and hanging drop vapour-diffusion methods, with a drop composition of 2 µl protein solution and 2 µl reservoir solution, equilibrated against 500 µl of precipitant solution in the well. The optimised crystallization condition was composed of 17.5 % PEG 3350 and 0.2 M NaCl (Figure 29A). The crystals appeared after one day with size dimensions of approximately 200 x 50 µm. However, the RuvBL1wt/RuvBL2-DII complex crystals did not diffract and could therefore not be used for structure determination. The other deletion complex composed of RuvBL1-DII and RuvBL2-DII crystallized under similar conditions and also contained PEG. Initial crystallization trials allowed to identify three promising hits in the pH Clear II Screen (QIAGEN): A9 (1 M $LiCl_2$, 0.1 M MES pH 6, 10 % PEG 6000), A10 (1 M $LiCl_2$, 0.1 M HEPES pH 7, 10 % PEG 6000) and A11 (1 M $LiCl_2$, 0.1 M Tris pH 8, 10 % PEG 6000). These drops had 1 M $LiCl_2$ and 10 % PEG 6000 as common features, but contained buffers with different pH values. Interestingly, no crystals grew in the wells A8 and A12 of the pH Clear II Screen which contained the same components as A9-A11, but had buffers at pH 5 and pH 9, respectively. These initial results were reproduced and optimised at the microliter scale using hanging drop vapour-diffusion, with a drop composition of 2 µl protein solution and 2 µl reservoir solution, equilibrated against 500 µl of precipitant solution in the well (Figure 29B). Before crystallization, 5 mM ADP were added to the concentrated protein solution in order to stabilise the complex. The best crystals were obtained with a reservoir solution of 0.8 M $LiCl_2$, 10 % PEG 6000 and 0.1 M Tris pH 7.5 (Figure 29C).

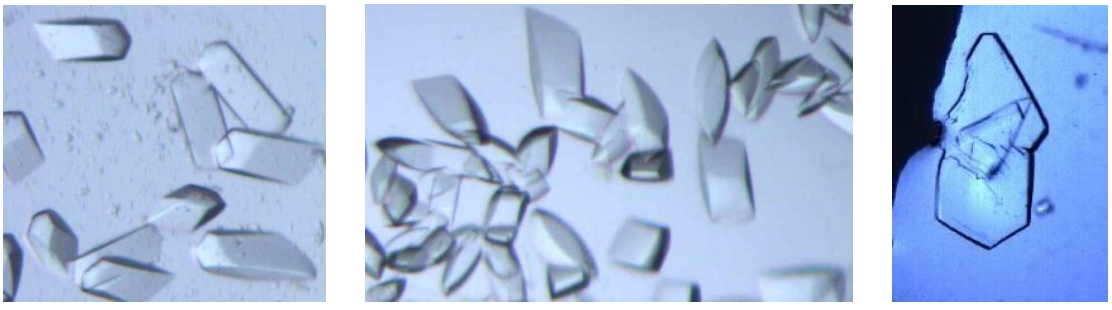

A) B) C)

Figure 29: Crystals of RuvBL1/RuvBL2 complexes with truncated domains II. A, RuvBL1wt/RuvBL2-DII crystals. B, RuvBL1-DII/RuvBL2-DII crystals and C, optimised RuvBL1-DII/RuvBL2-DII hexagonal plates used for structure determination.

One crystal obtained under these conditions diffracted to 4 Å resolution and was used to measure diffraction data leading to structure determination (Figure 30). The data set was collected at the ESRF in Grenoble at beamline ID14-2 using an ADSC Quantum 4 detector.

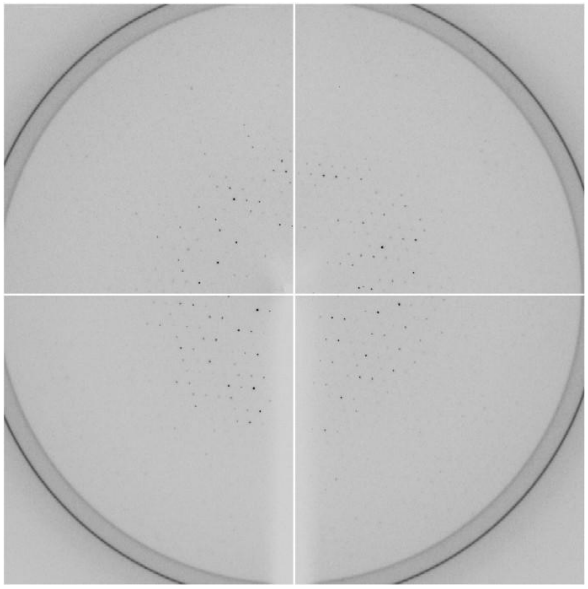

Figure 30: Diffraction pattern of the RuvBL1-DII/RuvBL2-DII complex. The crystal diffracted to 4 Å resolution. The ring surrounding the diffraction pattern may be due to unintentional freezing and thawing of the crystal in the loop and may prevent seeing spots at a slightly higher resolution of about 3.5 Å.

		RuvBL1-DII/RuvBL2-DII
Data collection		
Space group		$P2_1$
Cell dimensions(Å)	*a*	108.5
	b	242.0
	c	108.6
	β	118.7°
Wavelength (Å)		0.933
Resolution (Å)		47.6-4.0 (4.19-3.97)
R_{merge}		0.122 (0.360)
$I / \sigma (I)$		3.5 (2.1)
Observations (unique refl.)		88409 (38654)
Completeness (%)		91.6 (92.3)
Redundancy		2.3 (2.2)
Estimated $B_{overall}$ ($Å^2$)		83.9
Refinement		
Resolution (Å)		47.6 – 4.0
No. reflections work		36711
R_{work} / R_{free}		0.317 / 0.346
R.m.s deviations		
Bond lengths (Å)		0.022
Bond angles (°)		1.892

Table 12: Data collection and refinement statistics for the RuvBL1-DII/RuvBL2-DII complex. Highest resolution shell is shown in parenthesis. R_{free} is calculated from a random sample containing 5% of the total number of independent reflections measured.

The crystal was a fragment of a thin (*ca.* 20 μm) hexagonal plate (Figure 29C) and belonged to the monoclinic space group $P2_1$ with unit-cell parameters a = 108.5 Å, b = 242.0 Å, c = 108.6 Å and β = 118.7°, with 12 molecules in the asymmetric unit. A summary of the data collection statistics is given in Table 12.

4.3.4 Structure of the RuvBL1/RuvBL2 complex

The crystal structure of the RuvBL1-DII/RuvBL2-DII complex was solved at 4 Å resolution showing a dodecameric structure with a central channel, where each monomer appears complexed with one ADP molecule (Figure 31A and B).

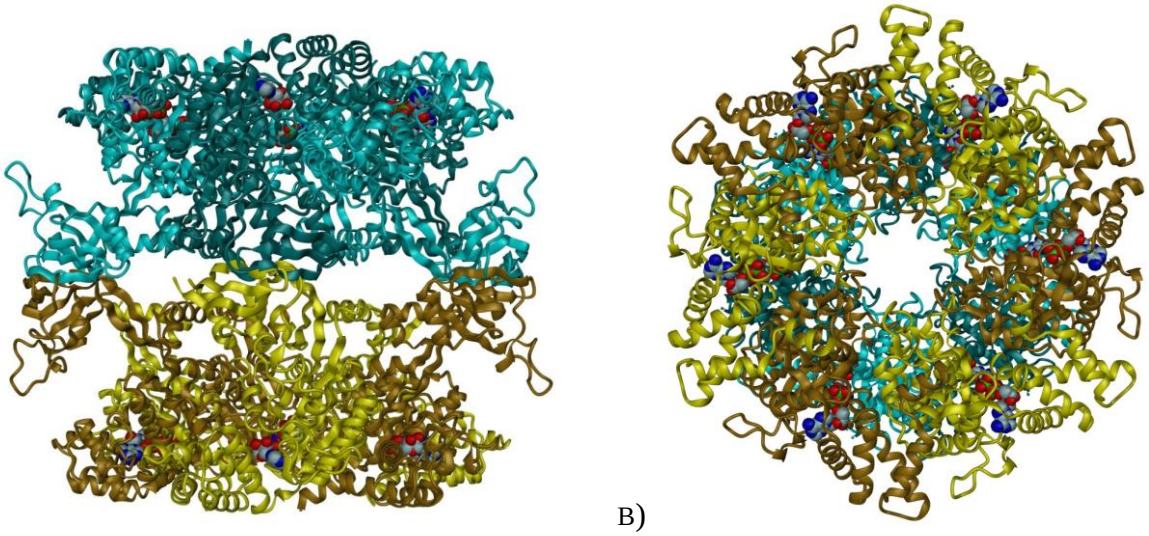

A) B)

Figure 31: The RuvBL1/RuvBL2 dodecamer. A, ribbon diagram of the dodecamer with missing part of domain II modelled (side view). Adjacent monomers are coloured cyan and dark cyan in the top hexamer and yellow and dark gold in the bottom hexamer. It is important to note that this colour scheme is used solely for clarity and does not imply alternating RuvBL1 and RuvBL2 molecules. The bound ADP molecules are depicted in space-filling mode, where each atom is represented by a sphere with a diameter twice its conventional van der Waals radius. Carbon, nitrogen, oxygen, and phosphorus atoms are coloured grey, blue, red, and green, respectively. B, ribbon diagram of the RuvBL1-DII/RuvBL2-DII dodecamer (bottom view). The colouring scheme is as in A. Drawings were prepared with DINO (Philippsen 2002).

As seen for the RuvBL1 structure, the central channel has an approximate diameter of 20 Å and the top and bottom surfaces (Figure 31A) appear to be remarkably flat. Surprisingly, the part of domain II that was not visible in the RuvBL1 structure (residues 248-276 in monomer A, 245-278 in monomer B and 247-276 in monomer C) represents the main interaction site between the two hexamers in the dodecamer and not the flat surface as expected. There was visible electron density in the map corresponding to that part of domain II (about 30 residues), but due to the low resolution data, it was impossible to model the C^{α}-chain. It can be speculated that this part of domain II, which was very flexible and therefore not visible in the RuvBL1 structure, becomes ordered and stabilised in the dodecameric complex of RuvBL1

and RuvBL2 showing electron density in the map. The reason for the stabilisation of this region may be its “zigzag”-like interaction between consecutive monomers in the dodecamer. Based on the RuvBL1 structure, the truncated part of domain II was modelled into the observed dodecamer of R1-DII/R2-DII and also seems to be involved in interaction between the hexamers (Figure 31A). Due to the high similarity between the two homologs it was not possible to distinguish between RuvBL1 and RuvBL2 monomers within the dodecamer. However, the two most likely possibilities are: one hexameric ring could consist of RuvBL1 and the other one of RuvBL2, or RuvBL1 and RuvBL2 monomers may alternate in both rings (Figure 32). Interactions between both hexameric rings are only mediated by domain II and must be divided into terminal part of DII interactions and internal part of DII interactions as shown in Figure 32.

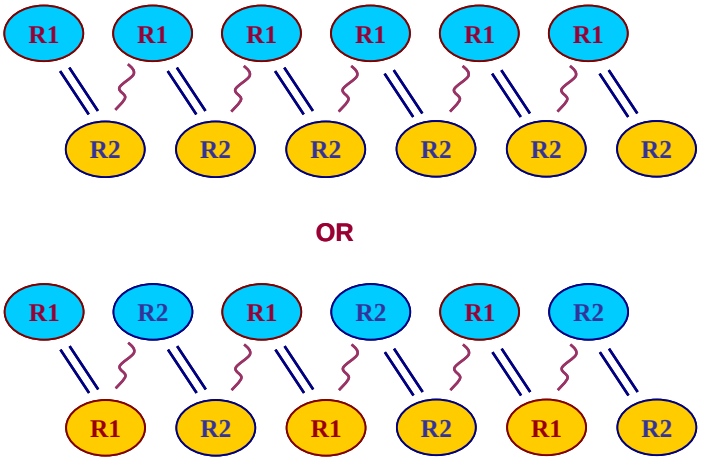

Figure 32: Scheme showing the two possibilities of RuvBL1 (R1) and RuvBL2 (R2) monomer distribution within the dodecameric complex. Interactions between both hexameric rings (blue and gold) are only mediated by domain II. Each monomer interacts with two neighbouring monomers from the other hexamer via terminal part of DII (represented by //) and internal part of DII interactions (represented by ⦚).

The domain II from each monomer from one hexamer (e.g. top, blue in Figure 32) interacts with two neighbouring monomers from the other hexamer (e.g. bottom, gold in Figure 32). Interactions occur between the terminal parts of DII truncated in the constructs used for crystallisation (represented by //) as well as the internal parts of DII containing helices and the stabilised region of domain II (represented by ⦚), which was not visible in the RuvBL1 structure (Figure 32). Of particular interest is the helix interaction marked in Figure 33.

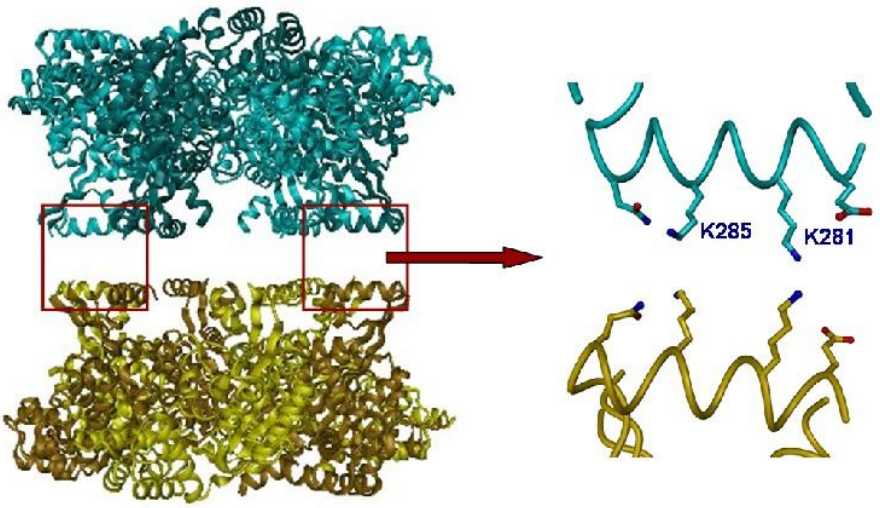

Figure 33: Helix-helix interactions between two neighbouring monomers in the dodecamer. The amino acid side chains involved in helix interactions are exemplarily shown for two interacting RuvBL1 monomers. Their positively charged Lys281 and Lys285 would probably repel each other.

In case of alternating RuvBL1 and RuvBL2 monomers in each hexamer it is very unlikely that RuvBL1 monomers may interact with each other through the highlighted helices (Figure 33) because their positively charged Lys281 and Lys285 involved in the helix-helix interaction (as shown in Figure 33) would repel each other. For that reason it is more likely that internal part of domain II interactions occur between RuvBL1 and RuvBL2 in opposite hexamers (as shown in Figure 32).

From the complex structure we learned that RuvBL1 and RuvBL2 monomers have a highly similar structure and for that reason the central channel of the hexamers formed by the single proteins should look almost identical. However, there would be a striking difference between the channel in RuvBL1 and RuvBL2 hexamers. The proposed DNA-binding loops in RuvBL1 containing the positively charged Lys107 and the negatively charged Glu342 are not present in RuvBL2, as these residues are both substituted by serines in the RuvBL2 sequence. This may be the reason for the different behaviour of RuvBL1 and RuvBL2 in nucleic acid-binding studies (see chapter 4.5.5).

4.4 Characterisation of RuvBL1 and the RuvBL1/RuvBL2 complex using small-angle x-ray scattering

The scattering of x-rays at small angles close to the primary beam provides low-resolution structural information on the overall shape of macromolecules in the absence of crystals. At the beginning of each experiment the sample was tested for aggregation caused by radiation

damage using multiple exposures of the same sample. The results showed no differences in the scattering from multiple measurements indicating that the samples did not suffer from radiation damage. In addition, measurements performed at different concentrations showed no effects upon the experimental data with the exception of RuvBL1 (Table 13). SAXS experiments require monodisperse protein solutions in order to obtain structural information. Due to the presence of double and single ring conformations modelling was not possible for RuvBL2, for the RuvBL1wt/RuvBL2wt complex and the RuvBL1-DII/RuvBL2-DII complex. However, using the calculated models from the monodisperse systems (RuvBL1wt and RuvBL1wt/RuvBL2-DII), the fractions of double and single ring conformations were calculated (Table 13) using OLIGOMER (Konarev et al. 2003).

Sample	Monomer	Hexamer	Dodecamer
RuvBL1wt (c < 6 mg/ml)	97	3	0
RuvBL1wt (c > 6 mg/ml)	3.2	96.8	0
RuvBL2wt (3.2 mg/ml)	0	45.9	54.1
RuvBL2-DII (0.9 mg/ml)	0	76.7	23.3
RuvBL1wt/RuvBL2wt (2.1 mg/ml)	0	28	72
RuvBL1wt/RuvBL2-DII (1.8 mg/ml)	0	1.3	98.7
RuvBL1-DII/RuvBL2-DII (0.9 mg/ml)	0	10.5	89.5

Table 13: Fractions of monomers, hexamers and dodecamers in solution of RuvBL1, RuvBL2 and their complexes. Different concentrations of each sample were measured (see chapter 3.17). The lowest concentration is indicated in parentheses. All fractions were calculated with OLIGOMER.

Interestingly, wild-type RuvBL1 at a concentration below 6 mg/ml was predominantly a monomer in solution. At higher concentrations RuvBL1 assembled into a hexamer. In contrast RuvBL2 only consisted of hexamers and dodecamers in solution at concentrations above 3 mg/ml (Table 13). A striking difference between RuvBL1 and RuvBL2 was the fact that RuvBL2 was able to form dodecamers beside the hexameric structures. Another interesting result is the composition of the RuvBL1/RuvBL2 complexes in solution. None of the complexes contained monomers suggesting that all RuvBL1 and RuvBL2 monomers were separated from the complex during purification and documenting that the complexes were very stable. As mentioned in chapter 4.3.1 the wild-type complex of RuvBL1 and RuvBL2 never crystallized. The composition of the RuvBL1/RuvBL2 complex solution may explain this negative result. Compared to the other complexes, RuvBL1wt/RuvBL2wt had the highest amount of hexamers (28 %) beside dodecamers (72 %) in solution (Table 13). In case only dodecamers are involved in crystal formation, the 28 % of hexamers would prevent crystallization by hindering an ordered packing of dodecamers to form a crystal. The crystal

structure of the truncated complex R1-DII/R2-DII showed that domain II was important for the interaction between two hexamers forming a dodecamer (Figure 31). In the wild-type complex the full-length flexible domains II may hinder association of all hexamers to form dodecamers. In contrast to this, the RuvBL1wt/RuvBL2-DII complex consisted almost completely of dodecamers (99 %, see Table 13). Also, the complex of RuvBL1-DII and RuvBL2-DII, which both have a truncated domain II, was composed mainly of dodecamers (90 %) and contained only 10 % of hexamers. Domain II might be more stabilised in the truncated complexes compared to the wild-type complex, thus improving the interaction of hexamers to form dodecamers.

The fits provided from the modelling using the RuvBL1 crystal structure and the experimental scattering curves were plotted. The calculated scattering from the crystal structure of RuvBL1 did not give an ideal fit to the experimental data, indicating that the conformation in the crystal may be affected by packing constraints. Fitting the experimental data using the ab-initio and rigid body modelling by DAMMIN and BUNCH respectively (Petoukhov and Svergun 2005; Svergun 1999) gave an improved fit to the data. Since proteins are more flexible in solution compared to the ordered molecules in the crystal structure, the proposed SAXS-model shows the average of all conformations in solution.

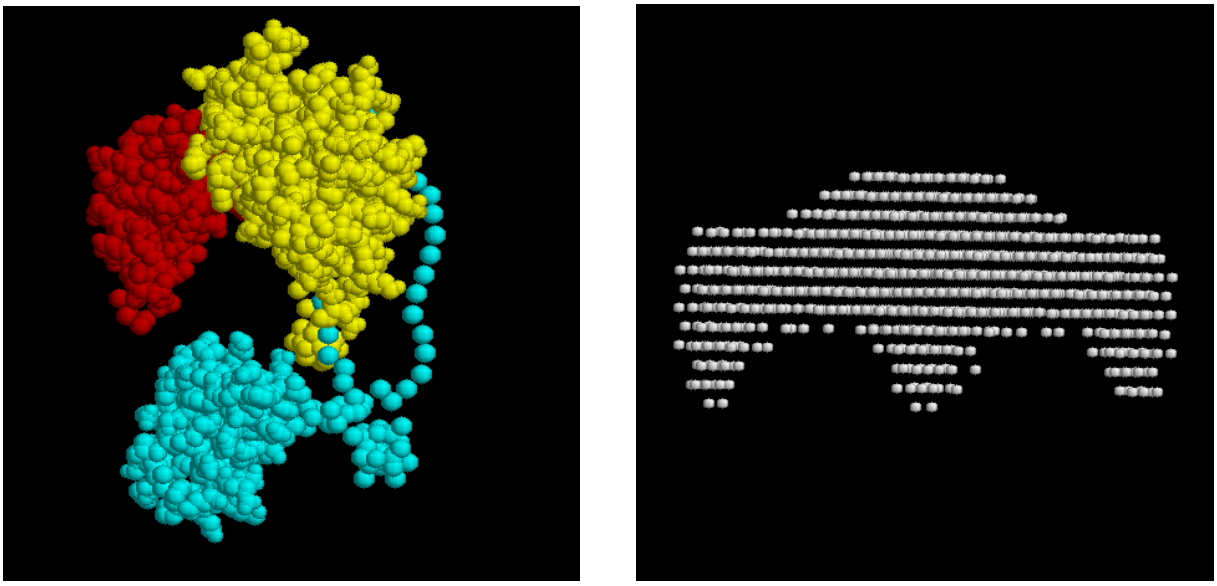

A) B)

Figure 34: SAXS models of RuvBL1. A, RuvBL1 monomer consisting of three domains coloured in yellow (DI), blue (DII) and red (DIII), respectively. B, ab-initio model of the RuvBL1 hexamer viewed from the side.

In agreement with the crystal structure, the SAXS results confirmed that there are three distinct domains in the RuvBL1 monomer (Figure 34A). However, the domains I and III are

more open in solution as shown by the ab-initio model. For that reason the surface of the hexamer is not as flat as in the crystal structure (Figure 34B, see Figure 15A for comparison with crystal structure). The ab-initio model shows spheres that do not represent atoms but indicate a region where the electron density corresponds to protein (Figure 34B).

An additional difference between the crystal structure and the SAXS results of RuvBL1 is the position of domain II. This domain is highly flexible in solution and the SAXS data show that it may be found within an extended area (Figure 35), while in the crystal structure its position is constrained by the interaction with neighbouring hexamers.

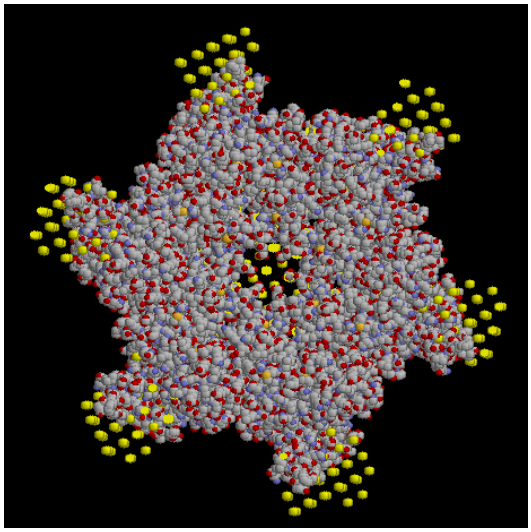

Figure 35: Domain II of RuvBL1 is more extended in solution compared to its position in the crystal structure. Superposition of RuvBL1 hexamers obtained from crystal structure determination (grey) and from ab-initio modelling using SAXS data (yellow).

4.5 Biochemical characterisation of RuvBL1, RuvBL2 and their complexes

4.5.1 ATPase activity of purified RuvBL1

Despite containing all the important structural motifs for ATPase activity (Figure 17), it was a surprising result that such activity was very low in human RuvBL1. Also, the ATPase activity was not stimulated by either single- or double-stranded DNA (Figure 36) or by RNA (data not shown). This was in contrast with the AAA^+ protein large tumour antigen of simian virus 40 (Sullivan and Pipas 2002), an hexameric helicase essential for viral DNA replication in eukaryotic cells (Borowiec et al. 1990), that was used as a positive control (Figure 36). The negative control RuvBL1_D302N contained a missense mutation in the Walker B motif (DEVH→NEVH), which was expected to abolish the ATPase activity of RuvBL1, and indeed exhibited no such activity (Figure 36).

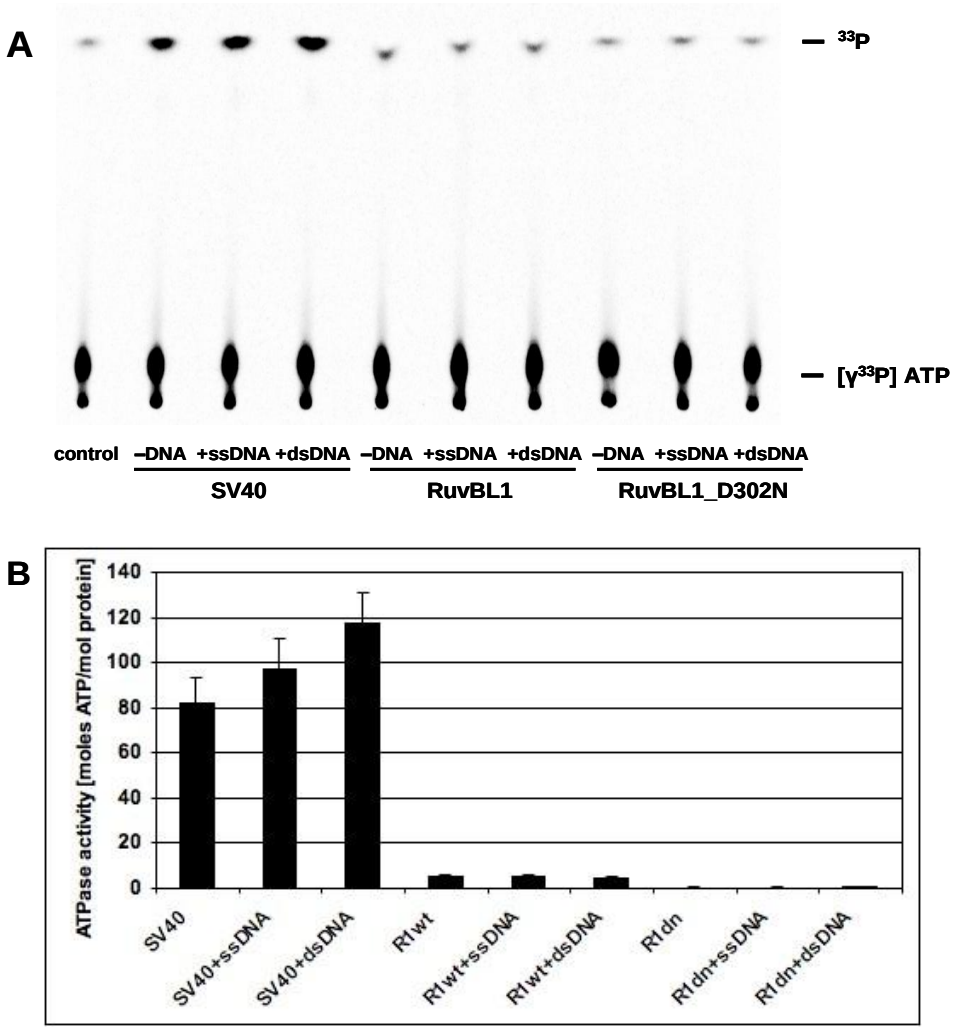

Figure 36: ATPase activity of purified RuvBL1. A, Free phosphate ^{33}P produced by hydrolysis of ATP was separated from [$\gamma^{33}P$] ATP by thin-layer chromatography. One representative experiment is shown. Free phosphate (fast migrating spot) and ATP (slowly migrating spot) were visualised by autoradiography. Note that a trace amount of free phosphate contaminated ATP (control). SV40 was used as a positive control and the Walker B mutant RuvBL1_D302N (R1dn) was used as a negative control. B, quantification of ATPase activity. Activity is expressed as moles of ATP hydrolysed per mole of protein. Reactions were incubated for 30 min at 37 °C. Bars represent the average of 5 independent experiments.

In an attempt to understand the weak ATPase activity of RuvBL1, a more detailed comparison between the nucleotide-binding pockets of RuvBL1 and of other AAA^+ proteins with known ATPase activity *in vitro* was performed. The compared nucleotide-binding pockets belonged to the AAA^+ domain of PspF (Rappas et al. 2006), RuvB (which by itself has only a low, RuvA-activated, ATPase activity) (Putnam et al. 2001), NSF-D2 (whose activity is regulated by soluble NSF attachment proteins) (Lenzen et al. 1998), SV40 large tumour antigen (Gai et al. 2004; Li et al. 2003), the E1 replicative helicase from Papillomavirus (Enemark and Joshua-Tor 2006), and the hexameric ATPase P4 of dsRNA bacteriophage Φ12 (Mancini et al. 2004). The results of this comparison are listed in Table 14 and show that RuvBL1 has the lowest solvent-accessible area among all these molecules, indicating a very tightly bound ADP

molecule. Therefore, it cannot easily exchange with ATP, and this may be the cause for the low *in vitro* ATPase activity of RuvBL1.

Molecule	PDB code	Location of ATP binding pocket	Ligand	Accessible area ($Å^2$)
RuvBL1	2C9O	DI/DIII interface	ADP	13.5
AAA+ Domain PspF	2C98	DI/DII interface	ADP	114.5
RuvB	1IN7	DI/DII interface	ADP	39.4
NSF-D2	1D2N	DI/DII interface	AMP-PNP, Mg^{2+}	55.7
SV40 LTag Helicase	1SVL	M/M interface	ADP, Mg^{2+}	37.4
Bϕ12 ATPase P4	1W44	M/M interface	ADP	90.1

Table 14: Characterisation of nucleotide-binding pockets in RuvBL1 and other AAA^+ proteins. The location of the nucleotide-binding pocket occurs either at the interface between two domains within a monomer (DI/DII or DI/DIII interface) or at the interface between two adjacent monomers in the hexamer (M/M interface). The solvent accessible area was calculated with NACCESS (Hubbard and Thornton 1993a), excluding the effects of water molecules present in the PDB file.

In addition, the adenine ring of ADP is held in place by a large number of hydrogen bonds and hydrophobic contacts, and both phosphate groups also have a large number of hydrogen bonds. The hypothesis of tight ADP binding is furthermore conveyed by the fact that helix α5 in DIII packs more closely against DI in RuvBL1 than the corresponding helix in DII against DI in RuvB. Hexamer formation does not appear to influence ADP binding, since the capping of the nucleotide-binding pocket by an adjacent monomer does not alter the solvent-accessible area calculations. However, it does obstruct a possible ADP exit channel and thus contributes to prevent the ADP/ATP exchange (Figure 16C). It can therefore be concluded that the ATPase activity of RuvBL1 which is necessary for several *in vivo* functions, very likely requires the presence of cofactors essential to promote ADP/ATP exchange.

4.5.2 Increased ATPase activity of the RuvBL1/RuvBL2 complex

The RuvBL1/RuvBL2 complex exhibited a significantly higher ATPase activity than the single proteins (Figure 37) suggesting that conformational changes within the complex allow an improved ADP/ATP exchange. Possibly RuvBL1 can act as a cofactor for RuvBL2 and vice versa. However, the ATPase activity of the complex is still much weaker than the activities of other AAA^+ proteins. Individual RuvBL1 and RuvBL2 had approximately three times lower activities compared to the complex. The ATPase activity of RuvBL2 and of the complex was also not stimulated by single- or double-stranded DNA (Figure 37). These results are in agreement with the data of Ikura *et al.* and Puri *et al.* who reported similar levels

of ATPase activities for the individual proteins and the complex (Ikura et al. 2000; Puri et al. 2007).

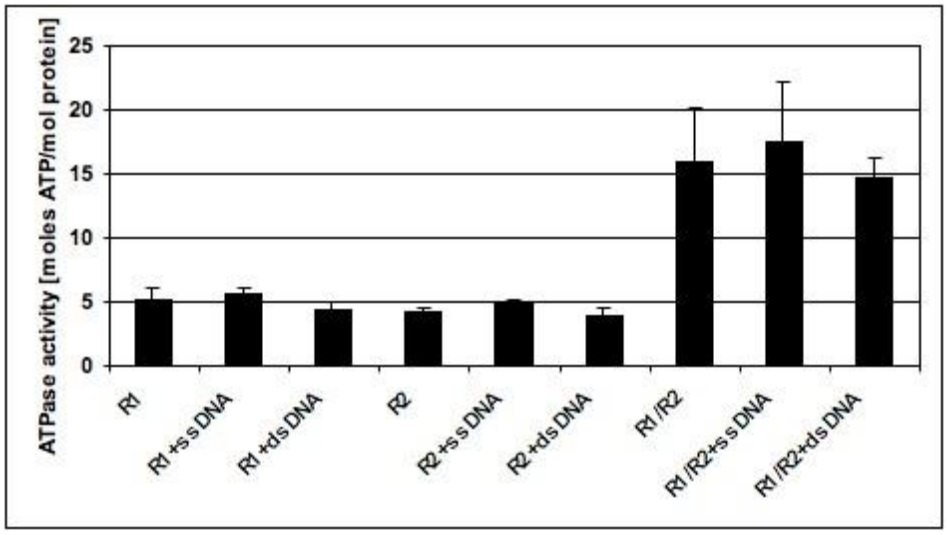

Figure 37: ATPase activities of RuvBL1, RuvBL2 and their complex. Quantification of activity is expressed as moles of ATP hydrolysed per mole of protein. Reactions were incubated for 30 min at 37 °C. Bars represent the average of 3 independent experiments.

RuvBL1 and RuvBL2 are mainly found as part of large chromatin remodelling or transcription complexes *in vivo*. Presumably, additional interacting proteins present in these complexes can further stimulate the ATPase activity of the RuvBL1/RuvBL2 complex.

4.5.3 ATPase activity of the RuvBL1/RuvBL2 complex is pH-dependent

Since many ATPases exhibit a pH-dependent activity, it was assumed that the ATPase activity of the RuvBL1/RuvBL2 complex can be further stimulated by changing the pH. In order to test that, buffers with different pH values were used in the assay.

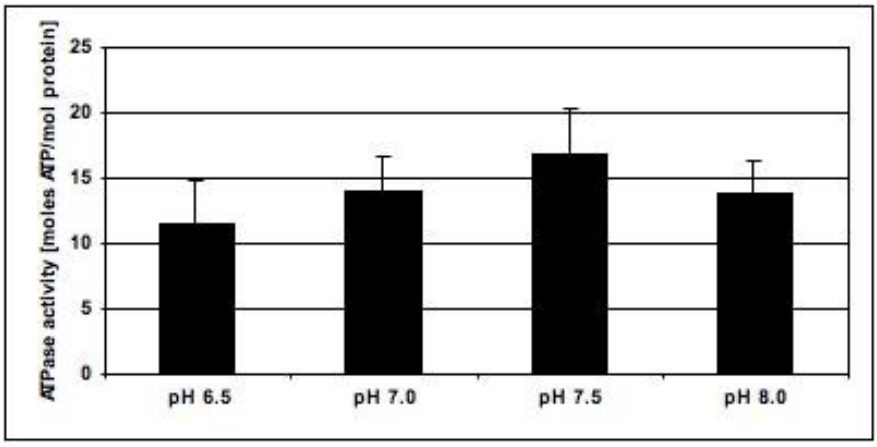

Figure 38: pH dependence of the ATPase activity of the RuvBL1/RuvBL2 complex. Quantification of activity is expressed as moles of ATP hydrolysed per mole of protein. Reactions were incubated for 30 min at 37°C. Bars represent the average of 4 independent experiments.

Indeed, the results showed that the activity of the complex was pH-dependent (Figure 38). The optimum pH value was 7.5, which was already used in the previous experiments and was therefore not modified.

4.5.4 Does domain II regulate ATP hydrolysis?

In order to demonstrate that the constructs with a truncated domain II do not lose their ability to hydrolyse ATP, all deletion mutants were tested for ATPase activity and compared with the wild-type constructs.

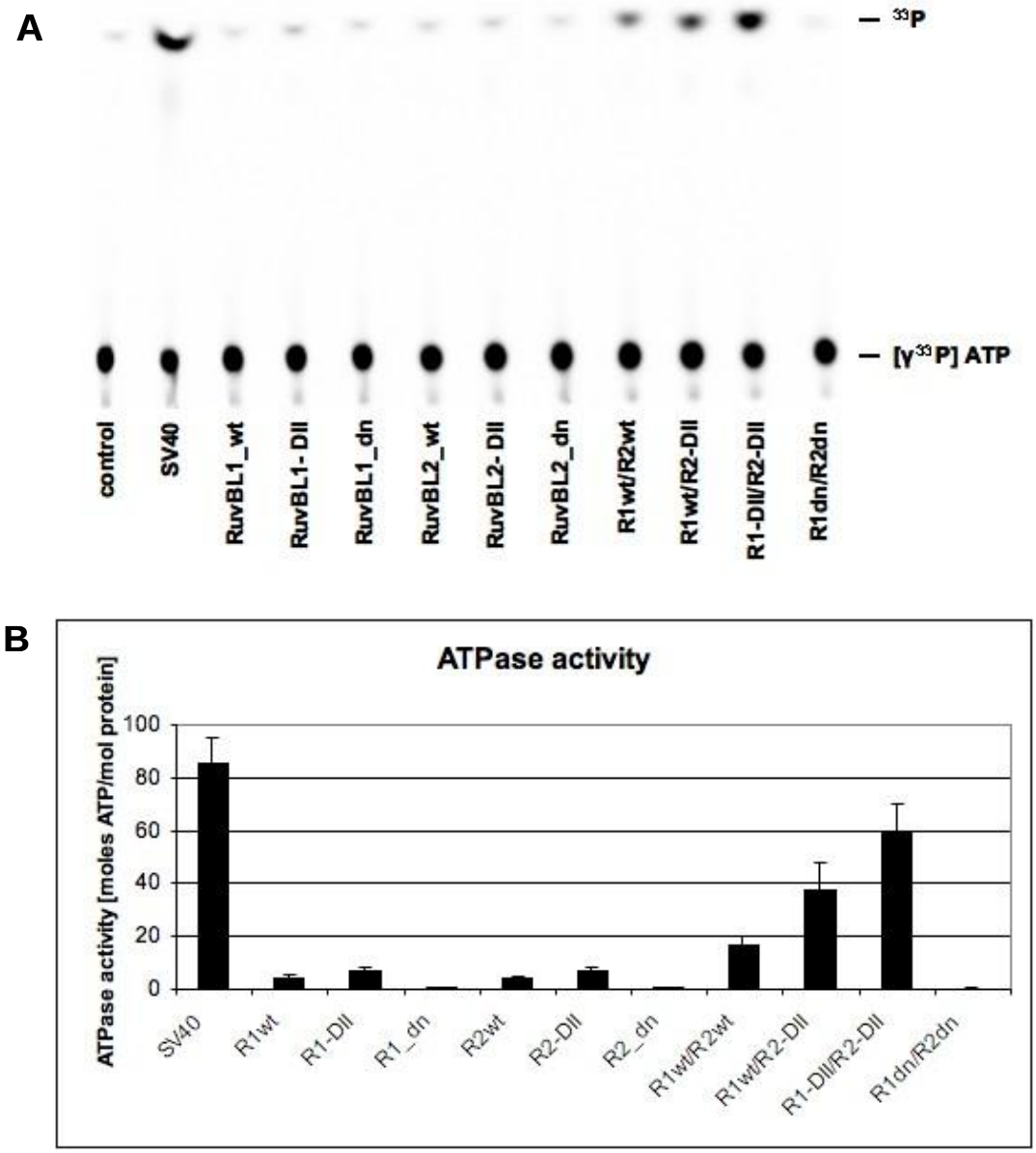

Figure 39: Significant increase of ATPase activity in complexes containing truncated domains II. A, Free phosphate ^{33}P produced by hydrolysis of ATP was separated from [γ^{33}P] ATP by thin-layer chromatography. One representative experiment is shown. Free phosphate (fast migrating spot) and ATP (slowly migrating spot) were visualised by autoradiography. Note that a trace amount of free phosphate contaminated ATP (control). B, quantification of ATPase activity. Activity is expressed as moles of ATP hydrolysed per mole of protein. Reactions were incubated for 30 min at 37 °C. Bars represent the average of 5 independent experiments.

Surprisingly, the RuvBL1/RuvBL2 complexes with truncated domains II exhibited the highest ATPase activities (R1wt/R2-DII and R1-DII/R2-DII, Figure 39). Also, the single proteins RuvBL1-DII (R1-DII) and RuvBL2-DII (R2-DII) having a truncated domain II showed an almost 2-fold increase compared to the activity of the wild-type proteins (R1wt, R2wt). As mentioned in chapter 4.5.2 the wild-type complex (R1wt/R2wt) had a three-fold higher activity than the single proteins hydrolysing 17 moles of ATP/mol of protein in 30 min. This activity was further increased to 37 moles of ATP in the complex of wild-type RuvBL1 and RuvBL2 with a truncated domain II (R1wt/R2-DII, Figure 39). In addition the complex of RuvBL1-DII and RuvBL2-DII (R1-DII/R2-DII), which also had a truncated domain II in RuvBL1, was even more active than the complex which contained only one deletion mutant. One mole of the R1-DII/R2-DII complex hydrolysed 60 moles of ATP exhibiting 70 % of SV40's (positive control) activity that hydrolysed 85 moles of ATP/mol of protein (Figure 39). These findings suggest that truncating domain II may mimic a similar *in vivo* situation, where cofactors present in the cell change the position of domain II by binding and clear the way to the nucleotide-binding pocket for a more efficient ADP/ATP exchange.

4.5.5 RuvBL1, but not RuvBL2 binds to nucleic acids

The diameter and the electrostatic potential of the central channel of RuvBL1 (Figure 16A and B) are indications that it may bind to single-stranded nucleic acids. The channel diameter of about 17.7 Å (measured between C^{β} atoms of Glu342) is comparable with the 18.2 Å value determined for the hexameric replicative helicase RepA (Niedenzu et al. 2001) (PDB 1GY8; measured between C^{β} atoms of Glu149) or the 20.7 Å value found for the hexameric ATPase P4 of dsRNA bacteriophage Φ12 (PDB 1W44; measured between C^{β} atoms of Asp240). It is also similar to the 18-20.2 Å range, which delimits the central channel in the E1 replicative helicase from Papillomavirus (PDB 2GXA) occupied by a single strand of DNA (Enemark and Joshua-Tor 2006). This diameter is in all cases too small for dsDNA to pass through.

Using an electrophoretic mobility shift assay, I showed that RuvBL1 binds to ssDNA and dsDNA as well as to ssRNA (Figure 40A). Given that the central channel seems to be too small to accommodate dsDNA, it is possible that a region outside of the ring makes DNA contacts. Based on this assumption and on the similarity between DII and the DNA-binding domains of other proteins, the 6xHis-tagged domain II of RuvBL1 (Leu122-Val238) was cloned, purified and used in electrophoretic mobility shift assay experiments. My results confirmed that domain II is a nucleic acid-binding domain (Figure 40A). Also, the results indicated that the labelled nucleic acids were specifically bound to RuvBL1 and domain II,

because they did not bind to the BSA protein used as control. To test whether RuvBL1 can bind to nucleic acids in a sequence-independent manner diverse substrates with varying sequences were chosen randomly. It was found that RuvBL1 shifted all nucleic acid substrates indicating binding in a sequence-independent fashion (Figure 40B).

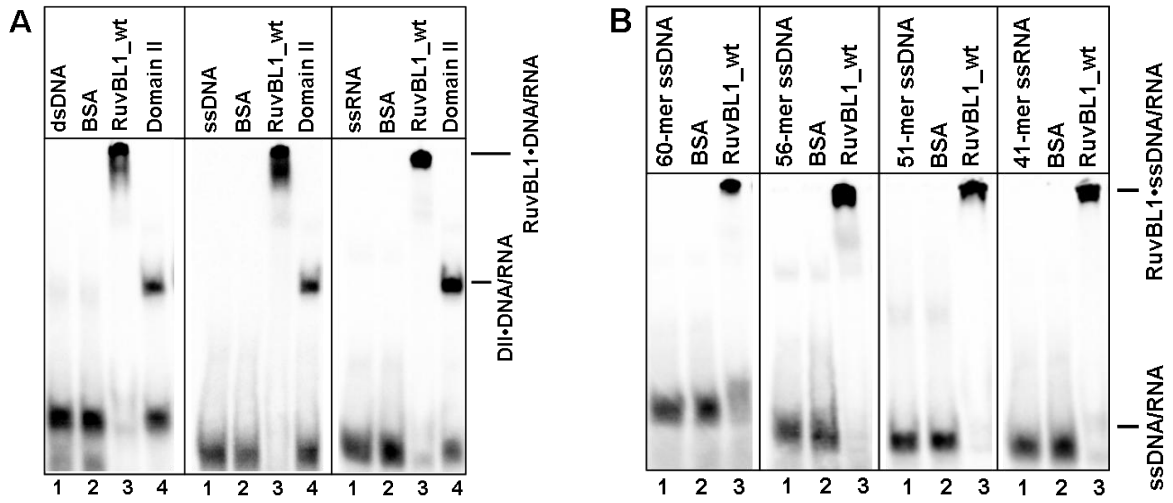

Figure 40: Nucleic acid binding to RuvBL1. A, dsDNA and ssDNA/RNA binding of purified RuvBL1 (lane 3) and domain II of RuvBL1 (lane 4) were tested using an electrophoretic mobility shift assay. Isolated DNA/RNA substrates were analysed (lane 1) to identify the positions of ssDNA/RNA and dsDNA, respectively. The BSA control (lane 2) was used to ensure that the nucleic acids specifically interacted with RuvBL1. B, further electrophoretic mobility shift assays with three different ssDNA substrates with diverse sequences and a ssRNA substrate to confirm nucleic acid binding to RuvBL1 (lanes 3) in a sequence-independent fashion. The samples were analysed on a 6 % non-denaturing polyacrylamide gel and visualised by autoradiography. The shifted protein-nucleic acid complexes are indicated.

In order to test whether RuvBL1 can bind to DNA in the absence of DII, the complete domain II was excised thus creating a mutant similar to RuvB, which does not possess this domain (see Figure 12). This deletion mutant was not soluble suggesting that domain II is important for proper folding and stability of RuvBL1. However, the soluble deletion mutants (see 4.3.2), which only had a truncated domain II were tested for ss and dsDNA as well as for RNA binding. Interestingly, RuvBL1 with the truncated DNA binding domain II still bound to nucleic acids (lane 5, Figure 41A and B) suggesting that the positively and negatively charged loops located at the top and the bottom of the central channel of the hexameric ring (Figure 16A and B) are also involved in nucleic acid binding. In addition RuvBL2 and the RuvBL1/RuvBL2 complexes were tested. Surprisingly, RuvBL1, but not RuvBL2 bound to nucleic acids (lanes 6 and 7, Figure 41A and B). Therefore RuvBL1 may be needed for DNA binding by the RuvBL1/RuvBL2 complex (R1wt/R2wt), which only had a weak affinity to nucleic acids (lane 8, Figure 41A and B). The RuvBL1wt/RuvBL2-DII complex exhibited marginal ssDNA binding (lanes 9, Figure 41A), whereas binding to dsDNA was increased

(lane 9, Figure 41B). The RuvBL1-DII/RuvBL2-DII complex did not bind to ssDNA (lane 10, Figure 41A), but shifted a little amount of dsDNA, as apparent by a weak band found in lane 10 of Figure 41B. In addition RNA binding of all constructs was tested (data not shown) but only RuvBL1 (see Figure 40) and the wild-type complex of RuvBL1 and RuvBL2 were able to bind to RNA.

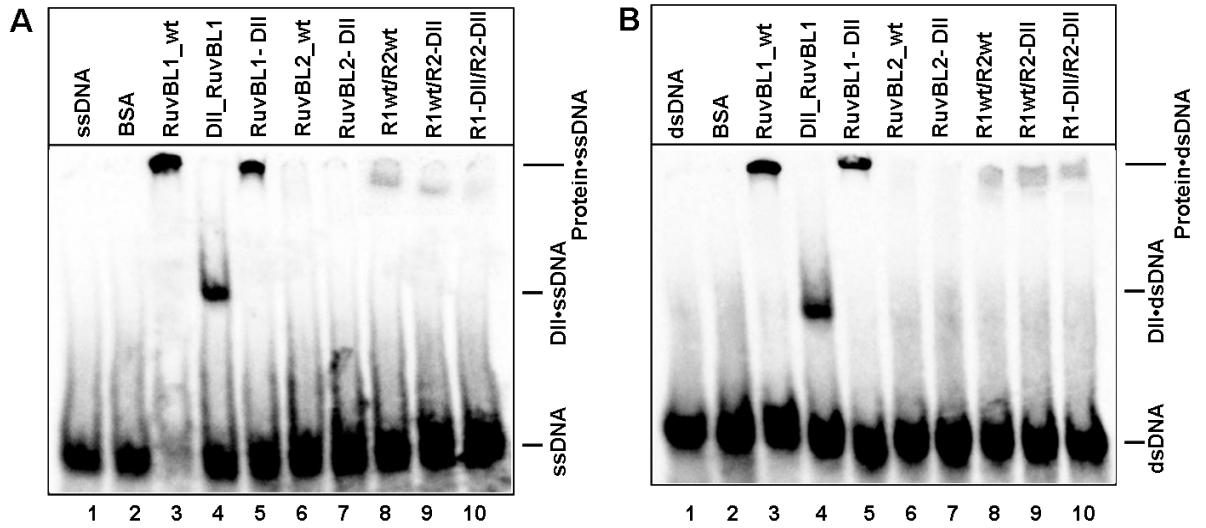

Figure 41: Nucleic acid binding to RuvBL1, RuvBL2 and their complex. Single- (A) and double- (B) stranded DNA binding of purified RuvBL1 (lane 3), domain II of RuvBL1 (lane 4), RuvBL1 with a truncated domain II (RuvBL1-DII, lane 5), RuvBL2 (lane 6), RuvBL2 with a truncated domain II (RuvBL2-DII, lane 7), the wild-type complex RuvBL1/RuvBL2 (lane 8) and the deletion complexes RuvBL1wt/RuvBL2-DII and RuvBL1-DII/RuvBL2-DII (lanes 9 and 10) were tested using an electrophoretic mobility shift assay. Isolated DNA substrate was analysed (lane 1) to identify the positions of ssDNA and dsDNA, respectively. The BSA control (lane 2) was used to ensure that the nucleic acids specifically interacted with the tested proteins. The samples were analysed on a 6 % non-denaturing polyacrylamide gel and visualised by autoradiography. The shifted protein-DNA complexes are indicated.

A possible explanation for the weak DNA binding of the RuvBL1/RuvBL2 complex is suggested by its three-dimensional structure. As shown in Figure 31A the domains II represent the interaction sites between two hexamers in the dodecamer. For that reason domain II within the complex is not completely accessible, as it is being covered by the adjacent monomer. Since this domain was shown to be important for nucleic acid binding in RuvBL1, the arrangement of domain II in the dodecamer of the RuvBL1/RuvBL2 complex could disturb its interaction with nucleic acids.

4.5.6 The highly conserved AAA$^+$ proteins RuvBL1 and RuvBL2 exert helicase activity

A 3' to 5' DNA helicase activity of RuvBL1 (Makino et al. 1999) and a 5' to 3' DNA helicase activity of RuvBL2 (Kanemaki et al. 1999) have been reported for the recombinantly

expressed proteins purified from bacterial cells. However, other groups failed to detect helicase activity for recombinant human RuvBL1 and RuvBL2 (Ikura et al. 2000; Qiu et al. 1998). To clarify this, not only 3' to 5' and 5' to 3' dsDNA substrates were tested but also substrates mimicking intermediates of transcription and DNA repair such as DNA/RNA hybrids and loop-forming dsDNA. However, no helicase activity was detected using purified human wild-type RuvBL1 and RuvBL2 (results are exemplarily shown for RuvBL1; Figure 42A and B) in agreement with the previously published data (Ikura et al. 2000; Qiu et al. 1998). The positive control used, SV40 large tumour antigen, was able to unwind all nucleic acid substrates (Figure 42) with the exception of the 5' to 3' DNA substrate shown in Figure 42B, confirming its unique 3' to 5' DNA helicase activity.

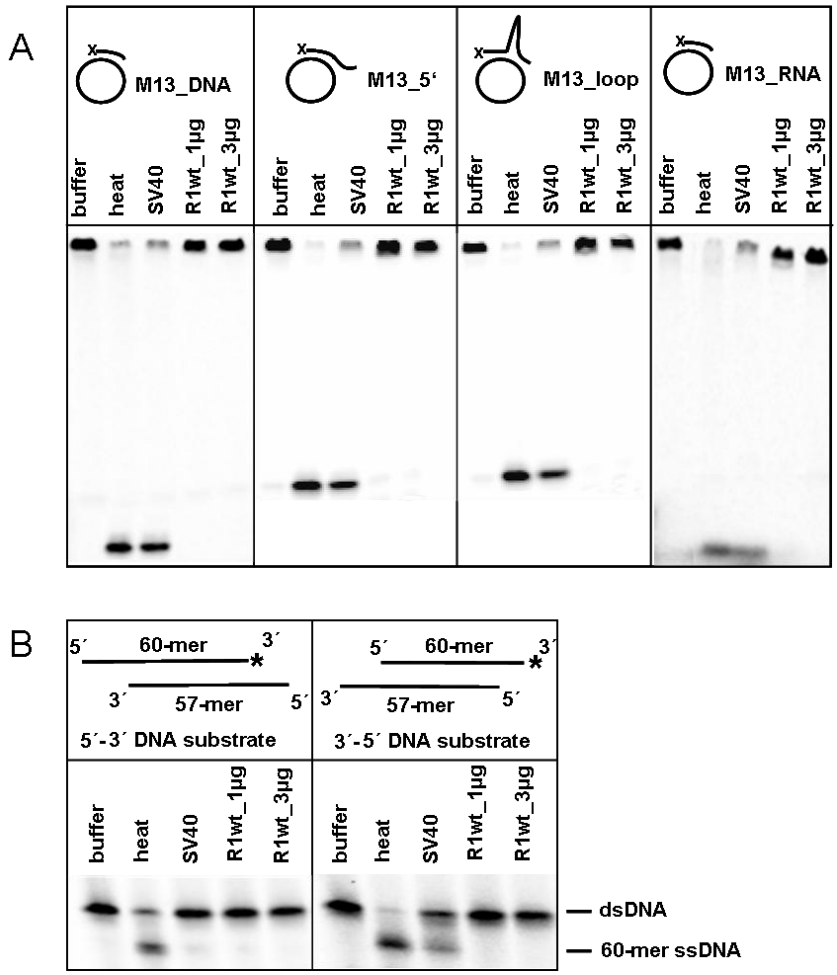

Figure 42: Lack of helicase activity in wild-type RuvBL1. Helicase activity assay of RuvBL1 using diverse M13mp18 DNA substrates (A) and 5' to 3' and 3' to 5' substrates (B). An asterisk denotes the ^{33}P label. DNA helicase activity was tested with 2 µg of the positive control SV40 large tumour antigen helicase (SV40) and 1 and 3 µg of wild-type RuvBL1 per reaction (R1wt). A boiled probe was used to identify the position of ssDNA (heat).

Helicase activity in hexameric AAA$^+$ proteins results from a mechanical motion derived from ATP hydrolysis. One essential requirement for the continued motion driven by the hydrolysis

of ATP is the rapid exchange at the active site between the hydrolysis products ADP + P_i and a new ATP molecule. In RuvBL1, hexamer formation and tight ADP binding appear to block the ADP/ATP exchange and thus severely lower its ATPase activity. On the other hand, hexamer formation seems to be crucial for ATP hydrolysis, because the essential residue Arg357, which is the likeliest candidate to act as an arginine finger, is provided by an adjacent monomer.

Since the complex of RuvBL1 and RuvBL2 exhibited an increased ATPase activity, it was possible that higher ATP consumption allowed the complex to exert helicase activity. The DII-truncation mutants were therefore also tested for helicase activity, in view of their unexpected high ATPase activities (see Figure 39).

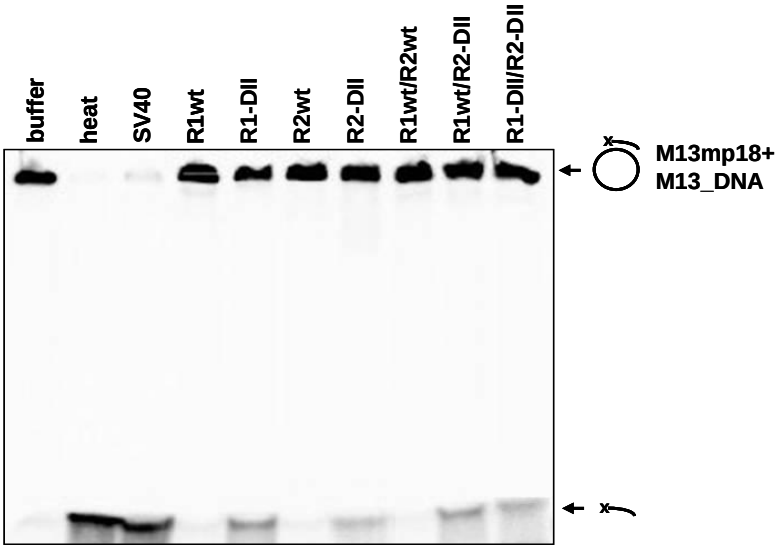

Figure 43: Helicase activity of the DII-truncated RuvBL1 and RuvBL2 mutants and their complexes. Helicase activity assay of RuvBL1, RuvBL2 and their complexes using a M13mp18 dsDNA substrate. An asterisk denotes the ^{33}P label. DNA helicase activity was tested with the wild-type proteins (R1wt, R2wt, R1wt/R2wt), the truncation mutants (R1-DII, R2-DII) and their complexes (R1wt/R2-DII, R1-DII/R2-DII). SV40 large tumour antigen helicase (SV40) was used as a positive control. A boiled probe was used to identify the position of ssDNA (heat).

As expected, none of the wild-type constructs R1wt, R2wt and R1wt/R2wt exhibited any helicase activity (Figure 43). This is in line with published literature relating that highly purified RuvBL1 and RuvBL2 do not possess helicase activity. Surprisingly I observed such activity when testing the deletion constructs. RuvBL1 containing a truncated domain II exhibited a higher helicase activity than its truncated homolog RuvBL2 (compare R1-DII and R2-DII in Figure 43). This may be due to their different behaviour in DNA binding. While RuvBL1 interacted with diverse DNA substrates, RuvBL2 did not bind to DNA under my assay conditions. However, it is possible that RuvBL2 can bind to other DNA substrates like

plasmid DNA used in the helicase assay. Unfortunately, binding of RuvBL2 to plasmid DNA could not be tested in the EMSA experiments because only smaller oligonucleotides were shifted in the gel.

In contrast to my expectations the complex of RuvBL1wt/RuvBL2-DII exhibited a slightly higher helicase activity than the complex of RuvBL1-DII and RuvBL2-DII. This was a surprising result, since the complex containing both deletion mutants exhibited a higher ATPase activity than the RuvBL1wt/RuvBL2-DII complex. For that reason one would expect also an increase in helicase activity when both RuvBL1 and RuvBL2 are truncated. The results of the nucleic acid-binding studies might explain these findings. RuvBL1, but not RuvBL2, bound to the tested nucleic acids. For that reason I assume that RuvBL1 was mainly responsible for DNA binding of the complex guiding it to the helicase substrate. Wild-type RuvBL1 had a higher affinity to DNA than its truncated version. That may result in a weaker binding of the RuvBL1-DII/RuvBL2-DII complex to the helicase substrate compared to the RuvBL1wt/RuvBL2-DII. Therefore the helicase activity of RuvBL1-DII/RuvBL2-DII could be weaker due to less binding of the complex to the substrate. Since the wild-type proteins exhibited no helicase activity *in vitro*, it can be concluded that cofactors binding to RuvBL1 and RuvBL2 in chromatin remodelling or transcription complexes alter the conformation of both proteins and allow them to exert their helicase activity.

4.5.7 Summary of biochemical results

Construct	ATPase activity (moles/mol of protein)	Helicase activity	DNA binding
RuvBL1wt	4.2	no	yes
RuvBL1-DII	7.3	yes	yes
domain II of RuvBL1	0	no	yes
RuvBL2wt	3.9	no	no
RuvBL2-DII	6.8	yes	no
RuvBL1wt/RuvBL2wt	16.9	no	yes
RuvBL1wt/RuvBL2-DII	37.3	yes	yes
RuvBL1-DII/RuvBL2-DII	59.4	yes	yes

Table 15: Results of ATPase, helicase and DNA binding studies showing all tested constructs.

Table 15 summarises the results of all biochemical assays. The wild-type proteins RuvBL1 and RuvBL2 exhibited only a marginal ATPase activity, which was almost two-fold increased in the deletion constructs. The ATPase activity of the RuvBL1/RuvBL2 complexes was significantly higher compared to the single proteins, while truncation of domain II within the

complexes enhanced the ATPase activity of the molecular machines even further. None of the wild-type proteins showed helicase activity. Conversely, the DII-truncated constructs were able to act as a helicase. This is a very interesting result because the scientific community already had doubts that RuvBL1 and RuvBL2 were able to exert helicase activity. EMSA experiments showed that only RuvBL1 bound to ssDNA, ssRNA and dsDNA in a sequence-independent manner. Also the purified domain II of RuvBL1, and RuvBL1 with a truncated domain II bound to nucleic acids suggesting that both the novel DII and the central channel of the hexameric ring were important for DNA binding. In contrast to RuvBL1, the RuvBL1/RuvBL2 complexes exhibited only a weak binding affinity to DNA, while RuvBL2 did not bind to the tested nucleic acid substrates.